# Microstructural, Mechanical, and Thermal Analysis of SS316L Weldment for Marine Engineering Application

*Dissertation submitted in partial fulfilment of the requirements*

*for the award of degree*

*of*

**Master of Technology in Marine Engineering & Management**

by

**ASWIN S KUMAR**

**(Reg. No. 2101215001)**

*Under The Guidance of*

**Dr. AMARISH KUMAR SHUKLA**

***Department of Marine Engineering***

**INDIAN MARITIME UNVERSITY**

**(A Central University, Government of India)**

Indian Maritime University, Kolkata Campus

Kolkata - 700088

July 2023

*Department of Marine Engineering*
**INDIAN MARITIME UNVERSITY**
**(A Central University, Government of India)**
**KOLKATA -700088, INDIA**

# CERTIFICATE

This is to certify that the thesis entitled **" Microstructural, Mechanical, and Thermal Analysis of SS316L Weldment for Marine Engineering Application "** submitted by **Mr. Aswin S Kumar (2101215001)** of the Department of Marine Engineering, Indian Maritime University (Kolkata Campus), in partial fulfilment of the requirements for the award of the degree of **Master of Technology** in Marine Engineering and Management, is a record of bonafide research work carried out under my supervision and guidance.

The content of the thesis does not form a basis for the award other degree to her at the best of my knowledge. In my opinion, the thesis is worthy of consideration for the award of the degree of **Master of Technology** in Marine Engineering and Management in accordance with the institute's regulations.

**Dr. Amarish Kumar Shukla**
Supervisor
Indian Maritime University, Kolkata campus
Kolkata – 700888, India

**Dr. Deepak Mishra**
Course coordinator (M.Tech)
Indian Maritime University, Kolkata campus
Kolkata – 700888, India

# COPYRIGHT AND CONSENT FORM

To ensure uniformity of treatment among all contributors, other forms may not be substituted for this form, nor may any wording of the form be changed. This form is intended for original material submitted to the Indian Maritime University, Kolkata Campus (IMU-KC), Kolkata and must accompany any such material in order to be published by the (IMU-KC). Please read the form carefully and keep a copy for your files.

**TITLE OF THESIS:** Microstructural, Mechanical, and Thermal Analysis of SS316L weldment for Marine Engineering Application.

**AUTHOR'S NAME and ADDRESS:** ASWIN S KUMAR, Sasi Bhavanam, Vallikunnam Po, kayamkulam, Alappuzha (Dist), Kerala, Pin - 690502, India.

# COPY RIGHT TRANSFER

1. The undersigned hereby assigns to Indian Maritime University, Kolkata Campus (IMU-KC), Kolkata, all rights under copyright that may exist in and to: (a) the above Work, including any revised or expanded derivative works submitted to the (IMU-KC), by the undersigned based on the work and (b) any associated written or multimedia components or other enhancements accompanying the work.

# CONTENT AND RELEASE

2. In the event the undersigned makes a presentation based upon the work at a conference hosted or sponsored in whole or in part by the (IMU-KC),the undersigned, in consideration for his/her participation in the conference, hereby grants the (IMU-KC), the unlimited, worldwide, irrevocable permission to use, distribute, publish, license, exhibit, record, digitize, broadcast, reproduce and archive; in any format or medium, whether now known or hereafter developed: (a) his /her presentation and comments at the conference; (b) any written materials or multimedia files used in connection with his/her presentation; and (c) any recorded interview him/her (collectively, the “Presentation"). The permission granted includes the transcription and reproduction of the Presentation for inclusion in products sold or distributed by (IMU-KC) and live or recorded broadcast of the Presentation during or after the conference.
3. In connection with the permission granted in Section 2, the undersigned hereby grants (IMU-KC) the unlimited, worldwide, irrevocable right to use his/her name, picture, likeness, voice and biographical information as part of the advertisement, distribution and

sale of products incorporating the Work or Presentation, and releases (IMU-KC) from any claim based on right of privacy or publicity.

4. The undersigned hereby warrants that the Work and Presentation (collectively, the "Materials") are original and that he/she is the author of the Materials. To the extent the Materials incorporate test passages, figures, data or other material from the works of others, the undersigned has obtained any necessary permissions.

# GENERAL TERMS

- The undersigned represents that he/she has the power and authority to make and execute this assignment.
- The undersigned agrees to indemnify and hold harmless the (IMU-KC) from any damage or expense that may arise in the event of a breach of any of the warranties set forth above.
- In the event the above work is not accepted and published by the (IMU-KC) or is withdrawn by the author(s) before acceptance by the (IMU-KC), the foregoing copyright transfer shall become null and void and all materials embodying the work submitted to the (IMU-KC) will be destroyed.
- For jointly authored works, all joint authors should sign, or one of the authors should sign as authorized agent for the others.

Signature of the Author

# SUMMARY OF CONTENTS

# ACKNOWLEDGEMENT

I want to take this opportunity to express sincere thanks and appreciation to everyone who helped me finish my project and create this project report. I extend my heartfelt thanks to RAdm. (Dr.) P J Rangachari, (Retd), our esteemed Director of IMU Kolkata Campus, for his unwavering support, encouragement, and provision of library and laboratory facilities for the preparation of this report.

I seize this opportunity to convey our deepest gratitude and utmost respect to my guide and mentor, Dr. Amarish Kumar Shukla, from the Department of Marine Engineering, for his exceptional guidance, diligent supervision, and constant motivation throughout the project's duration. His invaluable support, immense assistance, wholehearted cooperation, and fruitful discussions throughout the semester are encapsulated within this dissertation.

I want to thank Dr. Deepak Mishra, the course coordinator, for his guidance, assistance, encouragement, and support in getting this project done.

Additionally, I would like to thank the Indian Maritime University Kolkata for their support and cooperation in making this research possible by providing the facilities and resources needed. The help they provided was crucial to the accomplishment of the project.

Lastly, I extend my thanks to all those who were involved, directly or indirectly, during the course of this project.

# DECLARATION

I certify that

a) The work in this thesis is original and was completed by me under the supervision of my supervisors.
b) No other Institute for any degree or certification has received the work.
c) In preparing the thesis, I followed the guidelines supplied by the institute.
d) I have followed the Institute's Ethical Code of Conduct's guidelines and conditions.
e) Whenever I employed content (data, theoretical analysis, figures, and text) from other sources, I credited them by citing them in the thesis text along with offering specifics in the references.

**ASWIN S KUMAR**

# LIST OF FIGURES

# LIST OF TABLES

# LIST OF ABBREVIATIONS AND SYMBOLS

AISI – American Iron and steel Institute

SS – Stainless Steel

FEM – Finite Element Model

SMAW – Shielded Metal Arc Welding

SEM – Scanning Electron Microscopy

ANSYS – Analysis System

EDS – Energy Dispersive Spectroscope

MIG – Metal Inert Gas

FEA – Finite Element Analysis

ACT – Ansys Customization Toolkit

CAD – Computer-Aided Design

GMAW– Gas Metal Arc Welding

GTAW– Gas Tungsten Arc Welding

OAW – Oxyacetylene Arc Welding

FCAW – Flux-Core Arc Welding

SAW – Submerged Arc Welding

Nd: YAD – Neodymium-Doped Yttrium Aluminium Garnet

FZ – Fusion zone

HAZ – Heat Affected Zone

DCEN – Direct Current Electrode Negative

DCEP – Direct Current Electrode Positive

AC – Alternating current

DC – Direct Current

AWS – American Welding Society

HRB – Rockwell Hardness Measured on B Scale

HV – Vickers Hardness

WZ – Weld Zone

WM – Weld Metal

MS- Mild Steel

UTS – Ultimate Tensile Steel

YS – Yield Strength

NDT – Non-Destructive Techniques

DT – Destructive Techniques

ABAQUS – Finite Element Computer Code

## SYMBOLS

T – Temperature

t – time

S – travel speed

V – voltage

I – Current

HI – Heat Input

L – length

q – Heat flux

$\sigma$ – Stefan-Boltzmann constant

K – Thermal conductivity

$\rho$ – Density

# ABSTRACT

A SS316L steel is known as a marine-grade material, which is frequently used in a shipbuilding structure and marine industries. In the present study, a shielded metal arc welding (SMAW) process was used for similar welding of SS316L steel plate with dimension of 60 mm x 60 mm x 2 mm. A two different electrode E316L-16 and E308L-16, welding currents of 70 A, 80 A and 90 A and constant voltages of 24 V has been used for weldment. The impact of electrodes and current on the microstructure and mechanical properties of welded specimens was thoroughly investigated. To evaluate the flaw in the fusion zone (FZ), a surface macrograph and microstructure were analysed using scanning electron microscopy (SEM). In order to study the surface characteristics and ascertain the elemental composition of the samples, energy dispersive spectroscopy (EDS) was used. The hardness tests have been carried out in the base, heat-affected zone, and fusion zone of the welded joint. Tensile tests were carried out to study the effect of heat input on the yield strength (Y.S), Ultimate tensile strength (UTS) and elongation of a welded sample. According to the microstructure results, as the heat input increases, the grain structure of the welded zone gets finer in comparison to the base material. A hardness and tensile result shows that the properties of electrode and applied current has an effect on the mechanical properties of the SMAW welded sample. The hardness of the fusion zone increases compared to base material. The hardness result shows that as the current increases from70 A to 80 A by using the electrode of E316L-16 the hardness increases from 214 HV to 223 HV while the hardness further decreases to 208 HV for 90 A. Similarly, for E308L-16 electrode the hardness increases from 190 HV to 218 HV, and further it decreases to 168 HV for the applying current of 70A, 80A and 90 A respectively. A tensile result shows that the UTS of the SMAW welded sample varies from 190 to 262 $N/mm^2$ compared to base material, i.e., 565 $N/mm^2$Furthermore, thermal analysis was performed using ANSYS software to look at the impact of heat input at various welding arc times and identify the temperature distribution on the plate across various regions. In addition, the effect of heat input on the microstructure behaviour were studied in detail.

The current thesis has been broken into six chapters. The first chapter presents an overview of steel welding and its applications in numerous fields. It also emphasises the distinguishing feature of the SMAW welded 316L stainless steel. Chapter 2 discusses the literature on various stainless steel processing processes, as well as the reported literature on the properties of 316L

stainless steel, such as microstructural, mechanical, and thermal analysis of steel using the ANSYS software tool, and their applications. This is followed by identifying gaps in the literature and developing targets for addressing the issues related with SMAW welded 316L stainless steel. The materials and procedures employed in the current study are described in Chapter 3. Furthermore, this chapter discusses the various characterization strategies used in the current work. SMAW welded 316L stainless steel results and discussion in Chapter 4. A detailed investigation on the influence of changing current and electrodes on the microstructure and mechanical properties of SMAW welded 316L stainless steel was also conducted. Furthermore, the ANSYS software tool was used to study the temperature distribution during the SMAW welded 316L stainless steel. The study's summary and results are detailed in Chapter 5. Finally, in Chapter 6, the future scope and additional possibilities of current research work on SMAW welded 316L stainless steel were thoroughly examined.

***Keywords:*** SS316L, Electrode Material, Shielded Metal Arc Welding, Microstructure, Mechanical Properties

# CHAPTER 1
# INTRODUCTION

## 1.1 INTRODUCTION

Stainless steels have excellent weldability, mechanical properties, and corrosion resistance at sea environment. Because of that it is widely accepted in several industries such as marine engineering, chemical processing plants, steam generator tubes, fusion plants, and nuclear reactors [1]. Stainless steel is distinguished by having a minimum chromium concentration of 10.5% and the potential for additional alloying elements and encompasses a wide variety of corrosion-resistant alloy [2]. The alloy's suitability for a given environment is determined by its crystallographic structure and the specific amounts of chromium and molybdenum present, which can vary across multiple grades of stainless steel [2]. Austenitic stainless steel is highly formable, weldable, non-magnetic, and ductile at cryogenic temperatures. It is categorized in two subgroups, i.e., the 200 series and the 300 series. The 200 series have a lower content of nickel and increased manganese content because of that it has a higher yield strength but a weaker corrosion resistance which restricts its application in a broad range. The 300 series, including Type 304 and Type 316, are mainly alloyed with nickel. and manganese and nitrogen is used to reduce the usage of nickel and it is widely used. 316 stainless steels, known as marine-grade stainless steel, demonstrates resistance to specific corrosive environments. In 316L, the "L" classification indicates that this grade of steel contains lower carbon content which helps to prevent stress corrosion cracking compared to regular 316 steel [3]. AISI 316L austenitic stainless steels (ASS) are extensively utilized in various manufacturing organizations due to their enhanced mechanical properties, exceptional resistance to corrosion, ease of fabrication, and good weldability. They find application in the construction of large structures, pipe systems, heavy plates, different types of boilers, pressure and marine vessels, tanks, large ships, heat exchangers, nuclear reactor equipment, pumps, valves, fasteners, paper/pulp industry, oil and gas industry, and the petrochemical industry, among others.

In manufacturing industries, welding is a crucial process which is widely employed to join metals either by using fillers or metals. Welding is a process used to join the two work piece surfaces together to form a single product. This process is utilized to metallurgically connect two metal pieces, effectively forming a unified metal piece. Welding's significance arises from

its ability to fabricate intricate geometries by constructing individual parts and subsequently assembling them through joining. There are numerous types of welding techniques, such as friction welding, laser welding, arc welding, metal inert gas (MIG) welding, oxy acetylene welding, TIG welding and Shielded metal arc welding (SMAW). SMAW is typically performed manually. According to the American Welding Society, common applications of welding encompass construction, pipelines, machinery structures, shipbuilding, job shop fabrication, and repair work [4]. Welding technology enables the creation of complex configured parts, with SMAW being one of the most commonly employed methods [5]. SMAW is a simple and affordable welding technique it is also known as "stick welding" or manual metal arc welding [6].

ANSYS is the software utilized for the analysis of mechanical product design and civil structure designs. It employs computer-based numerical techniques to address various problems and is specifically known as Finite Element Analysis (FEA) software which is developed by ANSYS Inc. It finds extensive application in the industry for analysing diverse solutions. Its capabilities encompass a wide range of problems, enabling engineers to tackle complex, highly nonlinear, and large-scale models. It serves as a valuable tool for simulating computer models of structures, electronics, and machine components, allowing for the analysis of strength, elasticity, and temperature effects. ANSYS Workbench system is predominantly employed for most of its simulations. Additionally, ANSYS also develops software for data management and backup purposes. The advantages of ANSYS include its ability to import diverse CAD geometries (both 2D and 3D) from various CAD software applications. It is equipped with advanced engineering simulation capabilities, ensuring accurate results. By utilizing specific inputs, ANSYS evaluates the behaviour of products in relation to physics, making it a versatile software for simulating interactions among different physics domains like dynamics, statics, and fluids. It can also import different geometric shapes from various CAD software platforms, utilizing them for simulation purposes [7]. In ANSYS, the transient thermal analysis comprises the solution of the heat conduction equation in conjunction with the energy equation. The heat conduction equation elucidates the flow of heat within the plate, while the energy equation factors in heat generation resulting from welding. In order to conduct a transient thermal analysis of a welding plate in ANSYS, the procedure involves the following stages: creating the geometry, defining material properties, generating the mesh, applying boundary conditions, and obtaining the solution. The current research employed the Transient thermal analysis technique in ANSYS, which is a computational approach utilized for simulating and examining the evolving thermal characteristics of a welding plate. This form of

analysis is essential for comprehending the heat transfer and temperature distribution throughout the welding process, as well as forecasting the thermal stresses and deformations experienced by the plate.

In the current work, an attempt was made to weld SS316L utilising the SMAW technique with changing current and electrode. Microstructure, mechanical, and thermal analyses were used to investigate the effect of process factors on weldments. To optimise the welding parameters, detailed microstructural and mechanical property characterizations were performed. Finally, ANSYS was used to investigate the effect of heat input, temperature distribution along the weld bead, and microstructure evaluation.

# CHAPTER 2

## LITERATURE REVIEW

Stainless steel has a density of 7.87 g/cm$^3$, and it exhibits multiple advantages including remarkable high-temperature resistance, corrosion resistance, and great mechanical qualities like high strength, elasticity modulus, toughness, and stress resistance [8]. The primary material under investigation in this study is 316L stainless steel, also referred to as marine-grade stainless steel. It is a high-quality metal alloy composed primarily of Iron, Chromium, Nickel, and Molybdenum. Due to its exceptional corrosion resistance, 316L stainless steel is the preferred option for applications in wet or corrosive environments [9]. In addition, it also has excellent durability, thermal conductivity, and electrical resistivity, these properties have contributed to its widespread utilization in various industrial applications. However, despite these desirable attributes and extensive industrial usage, austenitic 316L stainless steel is nevertheless vulnerable to intergranular corrosion damage and pitting corrosion, especially in very corrosive settings. It is commonly employed as a metallic structure in industrial equipment such as food processing, petrochemical applications (atmospheric distillation overhead systems), domestic use, marine applications, shipping, and heavy-duty applications [10]. Austenitic 316L is highly regarded for its exceptional performance in industrial settings against corrosion reactions. It possesses unique alloys that set it apart from other types of steel used in industrial applications. Compared to austenitic 316, austenitic 316L is characterized by lower carbon content, denoted by the "L," which imparts increased strength and enhanced corrosion resistance [10]. The chromium content in 316L ranges from 16 to 28%, contributing to its improved resistance to corrosion damage [10]. Chromium also promotes passivation, and a chromium weight content of approximately 11% is necessary to achieve permanent stability of the passive layer that protects the surface of 316L stainless steel from general corrosion damage. The mechanical qualities of the steel, such as ductility, strength, and rigidity, are improved by nickel, which, unlike chromium, enables the steel to function effectively at high temperatures. Nickel also protects surfaces from corrosion damage and pitting. [10]. Molybdenum strengthens 316L stainless steel and increases its resistance to corrosion. It greatly increases resistance to pitting corrosion, especially in chloride conditions, and protects the steel's surface's existing thin passive film layer from oxidation effects.

## 2.1 Different Welding Techniques

These are some common welding techniques used in shipbuilding and marine industry [11].

1. Submerged arc welding
2. Gas metal arc welding (GMAW)
3. Gas tungsten arc welding (GTAW)
4. Oxyacetylene welding (OAW)
5. Flux Core - Flux-cored arc welding (FCAW)
6. High-energy welding processes such as Laser welding
7. Shielded metal arc welding (SMAW)

### 2.1.1 Submerged Arc Welding

Submerged arc welding (SAW), an automated method of arc welding, was among the earliest processes to undergo automation. It utilizes a continuous bare wire electrode that can be reused, with the arc protected by a layer of granular flux. The electrode wire is supplied into the welding arc automatically from a coil, while the flux is fed into the joint by gravity just before the arc is formed. By completely submerging the welding process, this technique eliminates common hazards such as radiation, sparks, and spatter that are often present in other arc welding methods. As a result, the welding operator employing SAW does not need to wear a bulky face shield, but they still need to wear safety glasses and gloves to protect their hands while working. [12]. The flux in close proximity to the arc melts during welding and combines with the liquid weld metal to eliminate impurities and create a glass-like slag on top of the weld joint. The unfused flux grains and the slag together offer the welded region good weather resistance and thermal insulation. Due to the delayed cooling process, excellent weld joints that are known for their strength and ductility are produced. The illustration demonstrates how the unused flux can be recovered and used again. However, the weld-covering hardened slag needs to be manually removed via chipping. To generate structural elements such as welded I-beams and the lateral and circumferential seams in large diameter pipelines, tanks, and pressure with vessels, submerged arc welding is frequently employed in the manufacture of steel. This method is frequently used to weld steel plates that are at least 25 mm (1.0 in) thick. High-carbon steels, tool steels, and the bulk of nonferrous metals cannot use; only low-carbon, low-alloy, and stainless steels can. Because gravity supplies the granular flux, the welding components must always be horizontal [12]. In the past Labanowski et al. [13] have conducted research into the joints' susceptibility to stress corrosion when they are welded in austenitic and

duplex steels, particularly in the context of building ship tanks for chemical transportation. Austenitic steels with the specification AISI 316 (316L and 316LN) were the primary materials utilised to build these tanks. High-yield welding techniques are extensively utilised in the naval construction sector, which is crucial for prefabricating big sections. One of the most frequently employed methods for welding thick plates is automatic welding with submerged arc welding. Although welding duplex and austenitic steels using this technique have several limits, it still offers excellent welding efficiencies and produces joints of good quality.

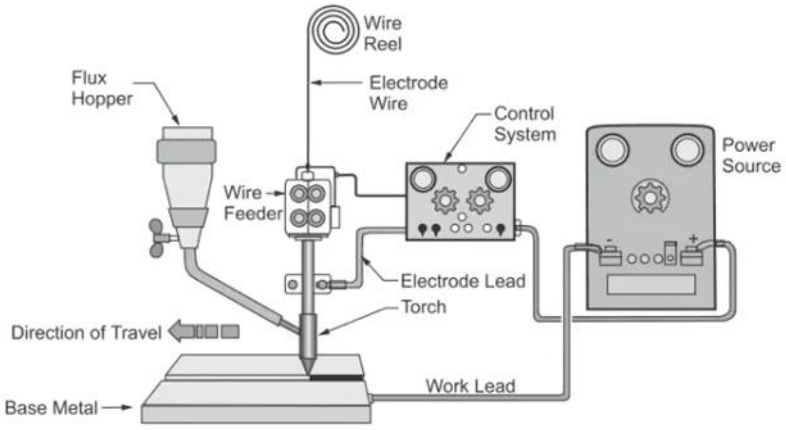


**Figure 2.1:** Diagram of the Submerged Arc Welding Procedure [14].

## 2.1.2 Gas Metal Arc Welding

When using a consumable bare metal wire electrode in gas metal arc welding (GMAW), the arc is protected by a gas. The welding gun automatically and continuously feeds wire from a spool. Depending on the ideal deposition rate and the thickness of the fragments that are joined, a wire diameter within 0.8 and 6.5 mm (1/32-1/4 in) might have to be employed [12]. Inert substances such as argon and helium, which as well as active gases like as carbon dioxide, are used as shielding gases. Other elements that influence the use of gases or gas combinations include the type of metal being welded. While the carbon dioxide is commonly used to weld low- and medium-carbon steels, inert gases work well for welding aluminium and stainless-steel alloys. By combining the bare electrode wire with shielding gases, the necessity for manual slag layer removal from the weld bead and grinding is removed. Therefore, numerous welding passes on the same joint can be done using the GMAW method [12]. As part of his study Ekaputra et al. [15] studied how the mechanical characteristics of 316L steel austenitic

material SS were affected by various welding speeds during GMAW. This sort of material is used in a wide range of items, such as nuclear reactors, valves and pumps, marine fittings, fasteners, pulp and paper manufacturing machines, and petrochemical sectors. They joined the 316L stainless steel for the study using the versatile, quick, economical, and high-quality (GMAW) procedure, also known as (MIG) welding. At various welding facilities, the GMAW process can be performed semi-automatically or automatically using a welding robot.

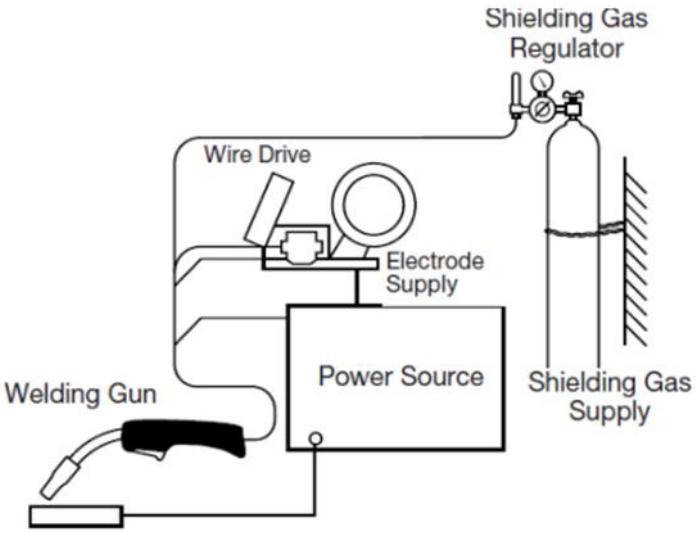


**Figure 2.2:** The Gas Metal Arc Welding Process is Shown in A Diagram [16].

### 2.1.3 Gas Tungsten Arc Welding

GTAW, commonly referred to as TIG welding, is a method of fusing and joining metals through the use of an arc created between a non-consumable tungsten electrode and the metals being worked on. To prevent overheating, the tungsten electrode is usually connected to a water-cooled copper tube, which is in turn linked to the welding wire [17]. The torch body and nozzle deliver a shielding gas (such argon or helium) to protect the weld pool from the atmosphere. Filler metal can be either manually or mechanically introduced to the arc when dealing with thicker materials. The electron emissivity, current carrying capacity, and contamination resistance of tungsten electrodes containing 2% cerium or thorium are superior to those of pure electrodes, producing a more constant arc. Since Ar is denser and provides more effective shielding than He, it is a more cost-effective alternative [17]. Azadkumar Vegda et al. [18] analysed and optimised the TIG welding process for SS 316L, a material that is often used in fabrication due to its strong weldability and low carbon content. The development of nuclear

fusion reactors, boiler parts and cryogenic structures all depend on the welding of SS-316L.The quality and strength of the weld are greatly dependent on the penetration, microstructure, mechanical characteristics, and residual stresses that are present during welding. The wrong choice of weld settings may result in system failure. The experiment covered several tests, and the analysis showed that welding factors including current, voltage, and filler material had a substantial impact on the weld joint.

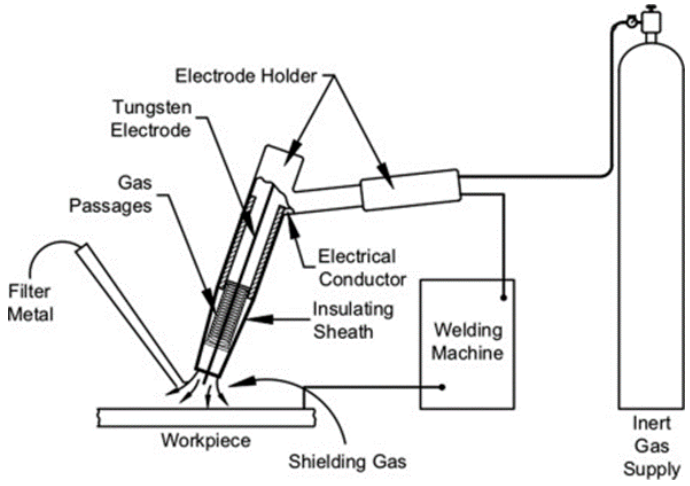


**Figure 2.3:** Process Flow Diagram for Gas Tungsten Arc Welding [19].

### 2.1.4 Oxy-Acetylene Welding (OAW)

The process of gas welding, also known as oxy-fuel gas welding (OFW), produces heat by burning fuel gas, usually acetylene, with oxygen [20]. The high flame temperature of acetylene makes it the preferred fuel gas for this process, leading to the alternative term oxy-acetylene welding. OAW uses oxygen and acetylene regulators, a torch, and gas mixing to completely melt the joint in order to achieve fusion. While acetylene is kept in cylinders packed with a range of 80 to 85% porous material, such as calcium silicate, and acetone to maintain a higher pressure, oxygen is kept in cylinders at pressures ranging from 13.8 to 18.2 MPa. However, acetone causes an unfavourable purple colour and lower flame temperature, thus measures must be made to prevent acetone and acetylene from combining during release. An alternative method is to use an acetylene generator, that consists of a water-filled cylinder and a valve that regulates the calcium carbide's passage into the water to make acetylene. The thickness of the metal being connected should be taken into consideration when choosing the OAW torch,

which should be held at an angle of between 30 and 50 degrees from the horizontal. At a distance of 1.5 to 3.0 mm, place the torch tip above the metallic plate with the white cone. The movement of the torch can be oscillatory or circular. When forehand welding, the torch is moved to the direction of travel of the tip. OAW does have some drawbacks, though, such as rougher weld lines that need more finishing for a neat appearance, significant heat affected zones surrounding the line of welding that affect the mechanical characteristics of the material, and the manual control that the welder must use to control torch movement and filler rod application [20]. Jakub Kowalski et al. [21] did research on the effects of straightening ship hull structures composed of 316L SS on their mechanical qualities and corrosion resistance. Determining the applicability of the flame straightening procedure for 316L steel ship constructions was the aim of his research. The tests were performed on 316L steel plates that had been flame heated. These plates are used often even in cold environments due to their excellent flexibility, adaptability, and corrosion resistance. They are frequently employed in shipbuilding to create RSW (refrigerated seawater) holds, which are used to carry fish in the water close to 0°C, and LNG petrol tanks, which operate at about 155°C.In the investigation, an oxyacetylene torch was used to hot straighten a 316L material plate, which is unusual for this kind of steel. The lack of a fair assessment of the stability of the heat treatment process and the achievement of the austenitizing temperature has been the primary factor in its limited utilisation. By employing water super saturation at 1100°C, the study aimed to achieve a single-phase austenitic structure with excellent corrosion resistance and no carbide precipitation in the steel. All three groups of test plates were put through a tensile test, which highlighted distinct variations in their mechanical characteristics. Particularly, the longitudinal direction showed a about 4% lower strength limit and a roughly 7% higher flexibility. The strength was about the same but slightly greater in the transverse direction of the reference plate in both heating settings, and the uncertainty for the tensile and an indication strength was calculated to be 0.27%, while the uncertainty for the elongation after fracture was 0.014%. Notably, fractures primarily occurred on the exterior or next to the burner's path. The hardness distribution of the examined objects' surfaces proved to be non-uniform and to have patterns in both situations. The hardness increased between the tracks, where the direct effect of the heat source was absent. This hardness distribution resembled a welded joint in that the heat impacted zone, particularly close to the fusion path, a region not directly affected by the heat source, showed a noticeable hardness increase. Notably, hardness levels measured 1 mm below the heated sheet surface showed noticeably less variation. Average hardness for sheets that were naturally chilled was 186.5 HV10, but it was 198.0 HV10 for sheets that were cooled in water. The

hardness distribution across the thickness of sheets that had been naturally straightened and cooled was almost symmetrical. However, the thermal process definitely had an impact on test plates that were cooled in a water bath because the distribution of hardness became asymmetrical and the minimum hardness plainly migrated towards the heated surface.

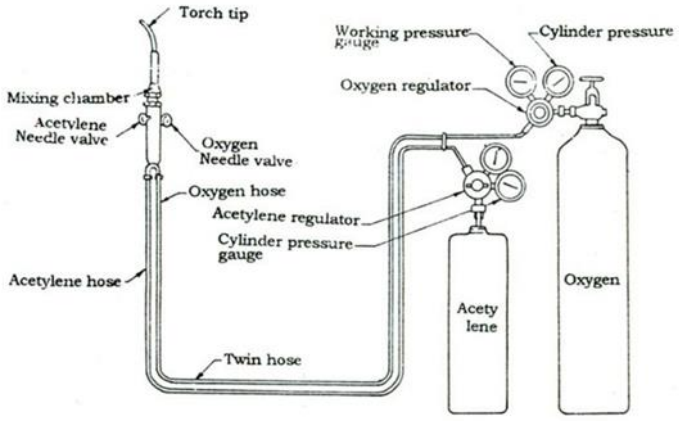


**Figure 2.4:** Schematic of Oxy-Acetylene Welding (OAW) Process [22].

### 2.1.5 Flux Core - Flux Cored Arc Welding

When using the flux-cored arc welding (FCAW) technique, the electrode is a continuous consumable tube having flux and other materials within. Deoxidizers and alloying components are examples of these extra additives. Due to its flexible tubular shape and delivery in coil form, the flux-cored "wire" can be continually fed through the welding arc gun. FCAW is available in two varieties: self-shielded and gas-shielded. The initially developed type of arc welding, self-protected flux-cored welding, gained its name because the arc was covered by a flux core. This FCAW type's core is made up of fluxes and other components that produce shielding gases to shield the arc. The creation of the second variety, gas-shielded flux-cored arc welding, used steel as its primary material. It depends on gases that are supplied from outside to shield the arc, similar to gas arc welding. welding with a flux core protected by gas, often known as this variation, is a hybrid of (GMAW) and (SMAW) since it uses an electrode with its flux in conjunction with separate shielding gases. For mild steels, carbon dioxide is a usual shielding gas, while a combination of argon and carbon dioxide has been used for stainless steels [12]. Ramazan Yilmaz et al. [23] The impact toughness and microstructural

properties of several weldments between AISI 316 L and AH36 steels were investigated using (FCAW). The major goal of the study was to look into the effects of different carbon dioxide ($CO_2$) ratios on the microstructure, impact toughness, and distribution of microhardness in the region between AH36 steel and the weld metal. The results revealed that as the $CO_2$ percentage of the shielding gas increased, the impact toughness of the weldment decreased. As the $CO_2$ level grew, the percent of ferrite in the weld metal dropped and the shielding gas composition influenced the microhardness data. Due of the inclusions in the weld metal, the transition zone between AH36 and the weld metal enlarged, lowering the notched impact toughness values. Flux-core arc welding (FCAW) has grown in renown due to its benefits, which include high deposits of weldable metal capability, suitability for automation, versatility in welding positions, ease of use, and cost-effectiveness for joining thick-sectioned materials in applications including chemical & cargo tanks in the construction of ships. The effects of shielding gas composition on weld metal microstructure, microhardness, and notched impact toughness were studied. The study includes employing the flux-cored with various shielding gas compositions to weld AH36 steel and AISI 316 L.

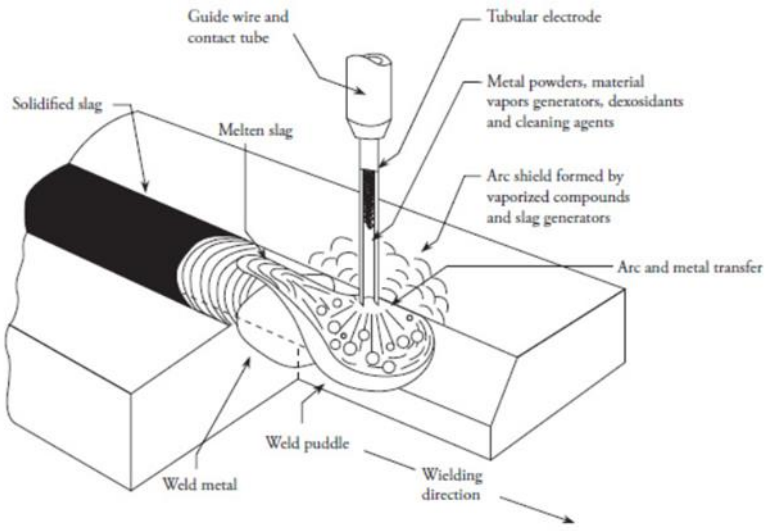


**Figure 2.5:** Schematic Diagram of Flux-Cored Arc Welding (FCAW) Process [24].

## 2.1.6 High Energy Beam Welding

Electron and laser beam welding are both high energy beam welding techniques. High-power laser applications are desirable because they can quickly weld the thin [25]. Laser welding has

several benefits, including smaller flange widths, greater structural strength, and automated processing at rapid speeds [26]. In the past, $CO_2$ lasers were commonly employed in automotive body applications. However, recent improvements in Nd: YAG laser science have made it possible for them to generate beam energies through optical fibre cables with capacities greater than 2 kW. This is particularly beneficial for robotic operations that call for leading the laser beam around fixed components. There are several different laser welding systems on the market right now, including those that are already used in industries that use $CO_2$ and Nd: YAG lasers. It is crucial to distinguish between heat conduction welding and deep penetration welding when employing laser beams for welding. At lower power densities or faster welding speeds, heat conduction welding occurs. A large and shallow pool of molten material is produced when the energy that was absorbed is transmitted into the volume of the workpiece. The laser beam is concentrated to a small point for deep penetration welding, and the power density can exceed $5x10^6$ watts/$m^2$. The laser beam is fully used, deep seams are produced, and absorption efficiency is increased. The amount of energy required to melt and vaporise a material is dependent upon its physical properties such as absorption coefficient, heat conduction, the wavelength of the light from the laser and the workpiece's surface traits.

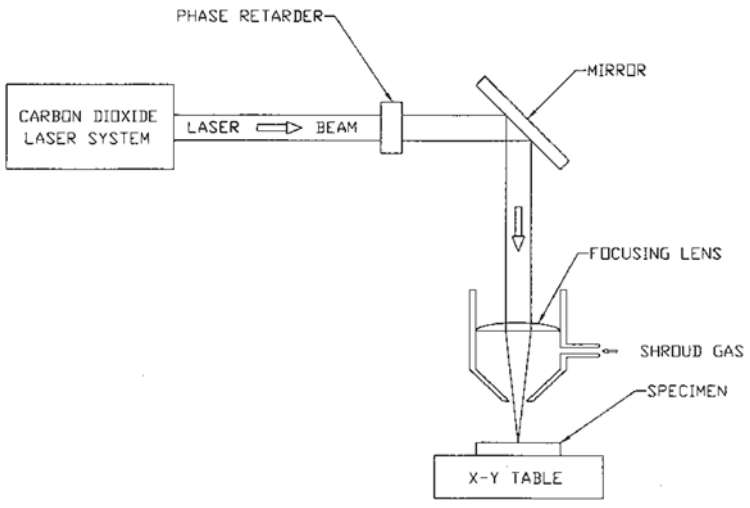


**Figure 2.6:** Schematic of Laser Welding Process [27].

A tiny heat-affected zone (HAZ), and deep, brittle, and slightly distorted weld profiles are typical outcomes of deep penetration welding. Due to its superior energy utilization and larger depth-to-width ratios, deep penetration welding is the primary [26]. Kumar et al. [28]

investigated the mechanical as well as microstructural characteristics of stainless steel 316L samples that were welded with a $CO_2$ laser and had a thickness of 8 mm. The welding procedure used 3.5 kW of power, 600 mm/min of speed, and shielding gas Argon. When the welded samples were examined, they showed excellent joints with full penetration and no discernible porosity or cracks. Impact fracture research discovered that the base metal had a higher energy absorption capacity (188 J) than the welded specimens (172 J). Tensile testing revealed that the weld joints had stronger strength values (600MPa) compared to the base metal (592 MPa), demonstrating that they were dependable. Additionally, the weld joints passed both the face and root bend tests without any obvious holes on the joint surfaces.

### 2.1.7 Shielded Metal Arc Welding

Shielded metal arc welding (SMAW), commonly known as stick welding, is a welding technique that utilizes heat to produce metal fusion. Heat is generated during this method by forming an electric arc between the surface of the base metal and the tip of a covered electrode. The SMAW technique employs welding technology to create an electrical circuit, which is accomplished by attaching a ground cable with a clamp to the workpiece and a welding cable with an electrode holder to maintain the electrode in place. When the electrode makes contact with the workpiece, it closes the electrical circuit, causing the electrode to melt and create the weld.

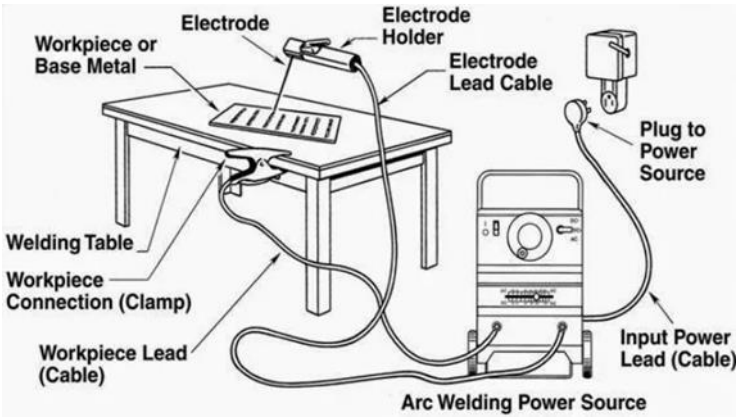


**Figure 2.7:** Shielded Metal Arc Welding Process Diagram [29].

The consumable electrode serves various purposes, including shielding the arc to prevent atmospheric contamination, modifying the mechanical properties of the welded metal to prevent excessive grain growth, and enhancing the weld's mechanical characteristics and

promoting the cleanliness of its surface. This welding technique is used in a variety of sectors, including maintenance and repair, shipping-related activities, pipeline installations, offshore development of platforms, and steel structure construction. It is appropriate for welding carbon steel, low and high alloy steel, stainless steel, cast iron, aluminium, nickel, and copper alloys. [11].

## 2.2 Shielded Metal Arc Welding Parameter Determination

### 1. Selection of Electrode Diameter

The electrodes utilized in shielded metal arc welding can be classified into two main types: joining electrodes and filler welding electrodes [30]. Depending on its intended application, joining electrodes are made specifically to join two metal pieces together, whereas filler welding electrodes are used to add material and fill gaps during the welding process. In contrast, classified based on various factors, including the strength of the weld metal, suitable welding positions, preferred current and polarity, and the type of coating, are the coated electrodes. The welding process employs a metal wire ranging from 1.5 to 6.5 mm in diameter and 20 to 45 cm in length. When selecting an electrode material, it is important to consider its desired qualities, such as high strength, ductility, and toughness. Shielded metal arc welding uses molten electrodes to both fill the welding region and produce an arc for the welding process. Various factors are considered when choosing the appropriate electrode, such as the material type, welding position, welding current, welding slot shape, and workpiece thickness. The electrode's diameter is adjusted based on the material thickness and welding slot design. In shielded metal arc welding applications, electrodes with core sizes of 2.50,3.25and 4.00 mm are commonly used [30].

**Table 2.1:** Various Workpiece Thickness and Their Respective Electrodes.

| Work Piece Thickness (D) | Electrode Core Diameter (d/mm) |
|---|---|
| D≤ 3 | 2.5 |
| 3 < D≤20 | 3.25 |
| D<20 | 4.00 |

The selection of welding current in Shielded Metal Arc Welding greatly impacts the rate of deposition, the size and shape of the weld bead, and the depth of penetration. In SMAW, it is

common to use direct current polarity with the electrode as positive, as this configuration delivers the highest heat input to the workpiece, allowing for greater penetration. When other welding parameters remain constant, increasing the current results in deeper and wider weld penetration, as well as larger weld bead size. Additionally, a higher welding current provides a larger weld pool, facilitating better fusion between the base metals [31].

2. **Welding Voltage**

The control of arc length (arc voltage) is crucial in SMAW, and it depends on various factors such as electrode composition, sizes, and welding technique. The arc length directly influences the arc voltage while these factors remain constant. Both high and low voltages have the potential to produce an inadequate circular section. Excessive spatter, porosity, undercut, and decreased convexity in fillet welds are all effects of excessive voltage. Conversely, extremely low voltage can result in the formation of pores and inadequate coverage along the edges of the welded area. Additionally, if a power source with a stable voltage is utilised, the welding current rises when the electrode feeding rate is raised and falls when the electrode speed is lowered, while all other variables stay constant. This factor is crucial for SMAW welding because it affects how quickly droplets move over the arc, which in turn dictates the type of metal transfer [31].

3. **Welding Speed**

The movement of the arc welding along the workpiece or the length of the weld seam formed in a certain time frame is referred to as welding speed. Slow welding speeds cause surplus weld metal to build up down the length of the unit, ultimately expanding the welding pool. As the weld metal accumulates and the heat input increases, the molten metal begins to move towards the front of the welding slot, causing disruptions to the formation of a stable arc. Conversely, raising the welding speed reduces the amount of heat delivered per unit length, resulting in a reduction in the volume of molten primary metal. This reduction adversely affects the wetting of the weld seam [30].

4. **Arc Length**

The occurrence of an arc depends significantly on the distance separating the electrode and the workpiece. Having a grasp of the concept of arc length is vital in diverse welding scenarios since it enables the differentiation of various arc lengths. The term "normal arc length" pertains to an arc length that matches the diameter of the electrode. On the other hand, a long arc occurs

when the arc length exceeds the electrode diameter, while a short arc length refers to distances smaller than the electrode diameter. Experience has demonstrated that arc blowing is more pronounced with a long arc length compared to a short one. As a result, using a small arc length for the task at hand is always advised [30]. Moreover, the arc blowing is reduced when welding with coated electrodes as opposed to uncoated or cored ones. Additionally, the blowing effect is more noticeable in thin coated electrodes compared to thick ones [30].

5. **Electrode Angle**

The electrode angle in Shielded Metal Arc Welding determines the weld quality and characteristics. It affects penetration, weld profile, heat distribution, and slag control. A steeper angle increases penetration and concentrates heat, while a shallower angle reduces penetration and distributes heat evenly. The shape and flow of the weld bead, along with the control of slag movement, are also affected by the angle [30].

## 2.3 Different Types of Currents

Welding utilizes three distinct types of electrical currents: direct-current electrode negative (DCEN), direct-current electrode positive (DCEP), and alternating current (AC) [32].

1. **DCEN (Direct Current Electrode Negative)**

In the direct-current electrode negative configuration, the electrode carries a negative charge, while the work is positively charged. From the electrode, electrons travel through the arc until they touch the surface of the metal being joined. Consequently, the electrode absorbs approximately one-third of the welding heat, leaving the remaining two-thirds to be transferred to the metal being welded. Formerly referred to as DCSP (direct-current straight polarity), DCEN welding current induces rapid melting of the electrode.

2. **DCEP (Direct-Current Electrode Positive)**

When using a direct-current electrode positive (DCEP), the work has a negative charge while the electrode has a positive charge. Consequently, the movement of electrons occurs through the arc, transferring from the electrode to the metal surface being welded. Due to the dispersion of electrons, the electrode receives approximately two-thirds of the welding heat and the weld metal receives the remaining third. Direct-current reverse polarity (DCRP), which used to be the term for this kind of current flow, is now more commonly referred to as DCEP. The best welding arc characteristics are known to be produced by DCEP current [32].

### 3. AC (Alternating current)

In an AC system, the electrons change direction every 1/120 of a second, causing the electrode and work to alternate between anode and cathode. This rapid reversal of current flow ensures that the welding heat is evenly distributed between the workpiece and the electrode, dividing the heat equally. As a result, a weld bead with both penetration and buildup is produced. The amount of buildup and penetration in the weld is affected by the heat applied to the electrode and workpiece. However, the choice of electrode also plays a role in determining the actual heat input to the metal being welded. A stronger arc that more forcefully fused with the base metal and produced a deeper weld in some circumstances was caused by a higher heat concentration at the electrode end. Therefore, just as choosing the right current type, choose the right electrode type is essential in defining the shape and penetration of the weld. [32].

## 2.4 Literature Review of Different Researchers

Several research studies have been conducted on materials, microstructural and mechanical properties, employing SMAW welding techniques along with other techniques. Various methods, involving different welding parameters, have been taken into consideration.

M. Mosaad (2020) et al. [33] Utilising the SMAW technique, it was investigated how the kind of electrode affected the welding properties exhibited by AISI 316 stainless steel. Around 30V voltage and 100A of steady current in reverse polarity were used to weld. Four passes were made at a speed of 8 mm/sec. Stainless Steel was welded in this study E312-17 and E316L-16 AWS electrodes. Figure 1.8 Show the macrographs of the welded specimens. Which showed complete penetration without any cracks or voids. The micrographs of fusion zones show a ferrite (dark) and austenitic (light) microstructure, along with coarse columnar grains. According to their findings, the welded specimen exhibited increased tensile strength, but the percentage of elongation in the welded sample was lower compared to the base alloy. Furthermore, the electrode used has an effect on the strength of the steel of the welded junction. Electrode E312-17 show higher tensile strength (950 MPa) and a lower elongation percentage (48%), while E316L-16 electrodes showed moderate tensile strength (850 MPa) and elongation percentage (52%). The fusion zone exhibited higher hardness values at its centre, with a gradual decrease observed along the specimens. E312-17 electrodes resulted in higher hardness (60.5 HRN) compared to E316L-16 electrodes (58 HRN). The heat-affected zone (HAZ) displayed a smaller grain size and greater hardness in compared to the base metal. Microstructure was

influenced by the cooling rates, wherein the weld zone experienced faster cooling, while the base metal underwent slower cooling. In general, the hardness measurements exhibited a declining pattern from the WM to the HAZ and finally to the base metal.

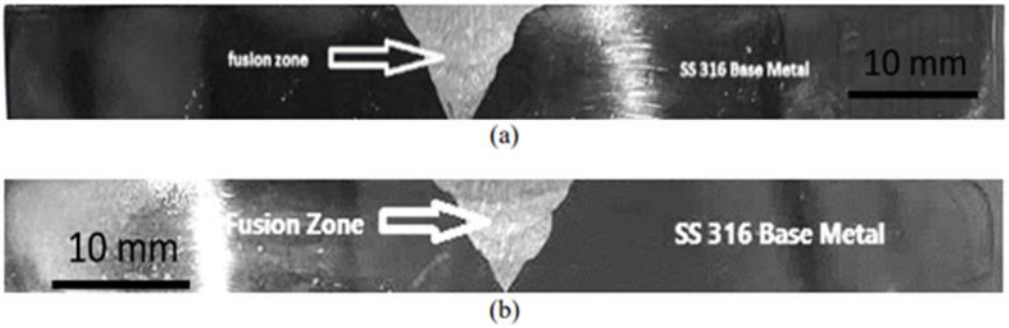


**Figure 2.8:** Macrostructure of (a) E312-17, and E316L-16 electrode [33].

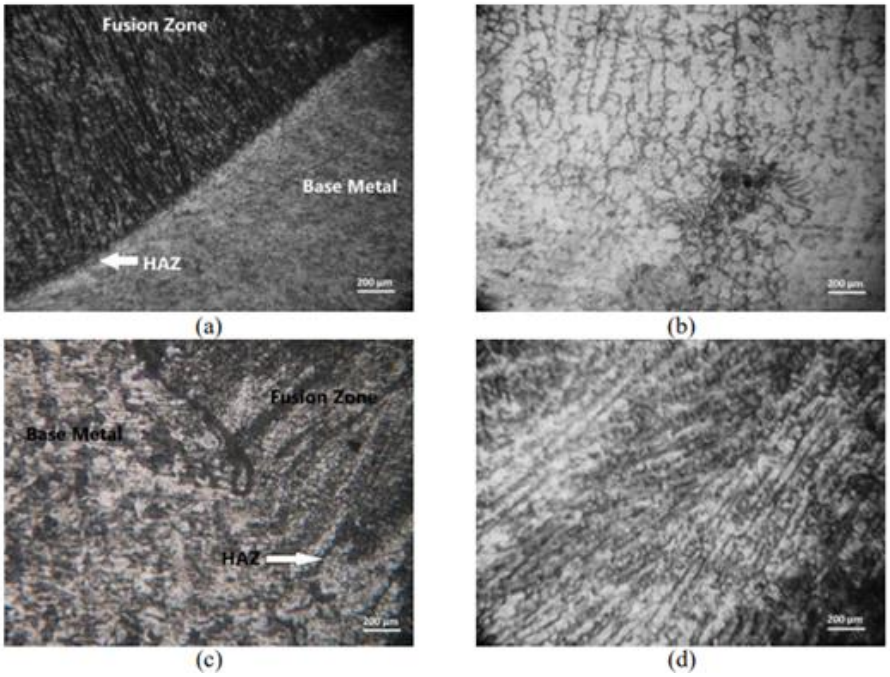


**Figure 2.9:** The micrographs display the Microstructure of SS 316 after welding using two types of electrodes: E312-17 (a, b) and E316L-16 (c, d) [33].

Salman et al. (2020) [34] examined the impact of the welding procedure and electrode composition on the corrosion properties. They were delivered for connecting, various electrodes were utilised. Using (SMAW) and (GTAW) procedures, two sets of samples were produced, consisting of AISI 304 & 316 stainless steel plates, respectively. E312-17 or E316L-16 electrodes were used in SMAW for AISI 304 SS, while ER316L or ER312 electrodes were utilised in GTAW. They examined the microstructures of AISI 304 stainless steel SMAW welds

made with E308L-16 & E312-17 electrodes and GTAW welds made with ER308L & ER312 electrodes in the (FZ) and (HAZ). GTAW FZs showed a cellular primary austenitic grain structure, while HAZ exhibited a coarser grain structure. In an austenite matrix, SMAW FZs displayed skeletal ferrite structure. Observation of AISI 316 stainless steel welds in the fusion zone and heat-affected zone revealed the use of E316L-16 and E312-17 electrodes for (SMAW) and ER316L and ER312 electrodes for gas tungsten arc welding (GTAW), respectively. In GTAW FZs, the presence of acicular ferrite within an austenite matrix was observed, while SMAW FZs using E312-17 exhibited a cellular austenitic grain structure, whereas those using E316L-16 electrodes displayed an equiaxed grain structure. The microstructures in the HAZ changed due to various factors such as temperature, heating rate, duration at elevated temperatures, and cooling rate.

Osoba et al. (2021) [35] conducted a research project examining the impact of heat inputs on the mechanical properties and weld profiles of carbon and stainless steel. Materials used in the study included steel with a low carbon content plates as well, 316 austenitic stainless-steel plates, 6 mm E7018 electrodes, and 6 mm, 308l-15 electrodes. The studies focused on integrating 316 austenitic stainless steel in a single V joint configuration with a consistent 3 mm root clearance. The welding process used was SMAW, with welding parameters set at 80A, 130 A welding currents, 20 V voltage, and welding speeds of 100 mm per minute. Heat inputs of 1.25 and 2.03 kJ/mm have been achieved as a result. The optical microstructures of the initial steel with low carbon and austenitic steel used were thoroughly examined in the study. In comparison to stainless steel, the steel with a low carbon microstructure had ferrite-ferrite boundaries of grain with carbide precipitates, however the stainless steel had a clean ferrite matrix. However, deformation was observed in the weld's microstructure, indicating that the applied heat input during the welding process caused a redistribution of the phase orientation. Microstructural analysis was used to identify the (HAZ) and (FZ) in the welds of low-carbon steel. The welds were created using heat inputs of 1050 and 2030 J/mm. The impact of welding current on microstructural inhomogeneity can be evaluated using this method. Different solidification routes and transformation sequences occur during steel welding, with the majority of welds commencing with the formation of ferrite and frequently followed by austenite nucleation on the ferrite grain boundaries. The existence of large ferrite grains in the heat-affected zone (HAZ) of the weld suggests that the cooling rates were inadequate when using high welding currents, resulting in the conversion of austenite into ferrite. There was detectable ferrite, its martensite, also and carbide precipitates in the HAZ of the 130 A weld,

while the fusion zone revealed particular microstructural characteristics such as martensite along the grain boundaries. Martensite development in the Heat affected zone indicated a quick cooling process during weld solidification. The study also examined the impact of welding current on the microstructure of stainless steel (SS). A welding current of 80 A and a heat input of 1.25 kJ/mm was utilized to create the weld. The microstructure analysis revealed that the fusion zone primarily consisted of columnar grains, while the heat-affected zone (HAZ) exhibited ferrite, grain boundary martensite, and some carbide precipitates. The hardness testing indicated increased hardness values in the HAZ, which were attributed to the presence of grain boundary martensite. Conversely, the weld fusion zone displayed equiaxed grains and inter-dendritic martensite, whereas the heat affected region of the weld produced with a higher welding current (130 A) exhibited coarse grain ferrite and grain boundary martensite. The presence of coarse grain ferrite in the HAZ, when compared to welds created with a lower current of 80 A and heat input of 1.25 kJ/mm, suggested slower cooling rates in certain parts of the HAZ. This slower cooling could potentially result in microstructural non-uniformity, which may adversely affect the material's strength. Increasing the heat input for welding low carbon and stainless-steel samples results in greater hardness in both the zone. In carbon steel, adding more heat causes both zones to become harder. However, no matter how much heat is applied, the hardness levels in the steel welds remain consistent. Stainless steel welds generally exhibit superior tensile properties compared to carbon steel welds, regardless of heat input, due to variations in alloy composition.

Wanees et. al (2020) [36] used the SMAW technique to complete identical welding joints on AISI 304 SS plates. They used reverse polarity constant DC welding current on a piece of metal that was 600 mm x 50 mm x 10 mm thick. The welding speed was 8 mm per second. The welding process was done in four passes. Two different electrodes, E312-17 and E308L-16, were used for welding AISI 304 SS plates. They discovered perfect penetration in the welded zone without any flaws, such as absence of fusion or the formation of voids, when they examined the microscopic image of AISI 304 SS that was welded together with the E312-17 electrode. The austenitic matrix in the fusion region of AISI 304 SS showed some acicular shape and a discontinuous network with vermicular ferrite structure, according to the microstructure of the region. In addition, coarse columnar dendritic crystals were seen at the fusion zone and along the direction of heat dispersion. Near the fusing line, there were heat-affected zones (HAZs). When the AISI 304 SS steel's mechanical properties were investigated, it was found that the welded joints' values for hardness, tensile strength, & elongation exceeded

those of the base material. Due to differences in alloying materials, microstructure, and grain sizes, the hardness was particularly higher in the fusion zone compared to the heat-affected zone (HAZ) and the base material. The choice of electrodes also influenced the hardness, with E312-17 exhibiting higher hardness than E308L-16. After reaching its maximum level, the hardness in the heat affected area starts to drop. The area of the HAZ next to the fusion boundary exhibits a finely textured composition and greater hardness, while the HAZ connected to the base metal demonstrates a coarser grain structure and reduced hardness, all within the welded portions. Unlike the vicinity of the base metal where cooling is slower, leading to a coarser grained microstructure, the HAZ regions neighbouring the weld/fusion zone experience rapid cooling rates. In general, the hardness data indicate that the trend is in the direction of declining hardness for base metal, weld metal, and HAZ. For E312-17, the hardness ranged from 53 to 59.5 HRN, while for E308L-16, it varied from 51.5 to 58 HRN. Moreover, the original alloy showed greater tensile strength and elongation percentage in its welded joints. When comparing the welded joints created with E308L-16 electrodes to those made with E312-17 electrodes, it was observed that the former had decreased strength but improved elongation. The initial alloy displayed a maximum tensile strength of 520 MPa and a 70% elongation rate. Following the welding process using E308L-16 electrodes, the tensile strength reached 845.8 MPa while the elongation rate decreased to 64%, while findings after welding with E312-17 electrodes were somewhat 927.08 MPa and 50.5%.

In a study conducted by Yousaf et al. (2021) [37] The three separate filler elements (E308, E309, and E316L) were employed to weld AISI 316L plates through the SMAW process. The study concentrated on the mechanical characteristics of welded AISI316L plates. To assess qualities including yield stress, UTS & (%) elongation, tensile tests were performed accordingly. According to the results, E308 filler material produced greater yield strength (3.66% greater than E309 and 3.94% greater than E316L), greater tensile strength (1.18% greater than E309 and 3.00% greater than E316L), and greater percent elongation (2.36% greater than E309 and 2.76% greater than E316L) in comparison to the other filler materials. Three distinct filler types E308, E309, and E316L were used in the hardness testing. According to the findings, E316L, E308, and E309 had the highest and lowest hardness values of AISI 316L ASS when SMAW welded. E316L, E308, and E309 each have a hardness value of 93HRB, 88HRB, and 84HRB, respectively. Similarly, Charpy V-Notch tests were performed using the same three filler materials at room temperature. The research results demonstrated that E308 exhibited higher impact properties than E309 and E316L, especially when measured

in terms of fracture toughness and fracture strength. In contrast to E309 and E316L, the fracture toughness and fracture strength of the E308 weldment are 8.27% and 7.86% greater, correspondingly. For example, for E308, the values were 141.12 J and 176.4 J/$Cm^2$, for E309 they were 130.34 J and 162.925 J/$Cm^2$, and for E316L they were 130.83 J and 163.5375 J/$Cm^2$.

Zumelzu et al. (1998) [38] research focused on examining how the microstructure affected the mechanical properties of welded joints made from 316 L stainless steel (SS). The presence of ferrite in the joints varied based on factors such as thermal contribution, WM, & welding process employed. Increasing the thermal contribution resulted in a higher ferrite content and a notable difference of 50% was observed when using type E 316 L-16 WM and the SMAW process. The tensile strength was directly influenced by the thermal contribution, as well as the chemical composition of the weld metal and variations in welding speed. To achieve consistent tensile strength, it was critical to discover any faults in the welding bead. Chemical differences caused the proportion of ferrite in the welding bead to go down. The best mechanical results were obtained for 316 L SS weldments by using type E 316 L-16 weld metal, a low thermal contribution of 15 KJ/cm, and a 5% ferrite content in the welded connection. The overall microstructure of the weld was defined by the process of solidification phase and subsequent solid-state transformation, according to SEM measurements. Fusion welding introduced modifications to the composition that affected the metallurgy and mechanical strength of the joint, highlighting the significance of controlling the weld metal type and welding arc energy to attain the desired attributes. Mechanical trials and SEM characterization proved helpful for evaluating and estimating the behaviour of welded joints in operation.

Choubey et al. (2014) [39] The investigation focused on studying the impact of heat input on the microstructure and mechanical characteristics of welded austenitic 202-grade stainless steel. The joining process employed was shielded metal arc welding (SMAW). They used a solid electrode filler called "AWS E308L-16" and tested three different heat inputs with voltage settings of 35 V and current settings of 75A, 100A, and 125A. The rate of welding was 2.50 mm per second, leading to heat inputs of 0.787 KJ/mm, 1.050 KJ/mm, and 1.312 KJ/mm consecutively. Microhardness was measured perpendicular to the base plate surface, showing varying values within the welded joint based on heat input. The top of the weld bead had the highest microhardness, decreasing towards the centre due to different cooling speeds. In the heat-affected zone, microhardness was highest for low heat input, followed by medium and high inputs. The base metal consistently measured at a specific microhardness value. The fusion boundary zone exhibited different microhardness values based on the heat input levels.

The existence of partially unmelted grains that serve as nuclei for new precipitating phases throughout the solidification process accounts for the elevated microhardness in the fusion boundary zone. The microhardness decreases in the HAZ after reaching its peak value, with the coarse-grained HAZ exhibiting lower microhardness and the fine-grained HAZ showing higher microhardness. Different cooling rates and microstructure in the HAZ and surrounding areas account for the observed trends. Order of joint hardness: weld metal, HAZ, base metal, fusion boundary. Higher heat input leads to grain coarsening in HAZ, backed by micrographs. Tensile strength: low heat input 640 MPa, medium heat input 605 MPa, high heat input 586 MPa. Elongation: low heat input 28.771%, medium heat input 24.450%, high heat input 20.083%. Lower heat input provides greater tensile strength and ductility due to smaller dendrite diameters and reduced inter-dendritic spacing in fusion zone. Higher heat input causes decreased tensile strength and ductility due to larger dendrite diameters and wider interdendritic spacing in fusion zone. In addition, the heat-affected region in all tensile specimens shows fracture. High tensile strength and ductility can be seen on the fractured surfaces of specimens made with low heat input, while dimples made with more heat provide coarser, longer fracture surfaces.

### 2.4.1 FEM Model for Predicting Thermal History

Miftin et al. (2020) [40] develop a dependable FEM model that can be used to predict the thermal history and residual stresses in welds of carbon steel pipes. The residual stress was measured at the welding centre using the hole drilling method and was found to be 611.78 MPa, which closely matched the predicted residual stress by the Ansys program. Due to material contraction during cooling, high residual stress was seen at the welding centre and increased in the areas nearby the weld. The numerical findings demonstrated steady residual stress distribution around the weld zone's centre, with a value of around 628.56 MPa, increasing towards the weld zone's interface with the heat affected zone, and peaking at about 747.59 MPa. Relative to the weld location, residual stress dropped quickly in the HAZ and fell to a minimum value of 50 mm. While there were some small discrepancies between experimental and numerical findings, they were reasonably close. These discrepancies could be attributed to differences in assumptions, simplifications, and uncertainties in measurement techniques. The position of the gauge for strain on the welded specimen and the non-smooth surface produced by welding may affect how precisely the residual stress measurements are made. However, the reproducibility of the experimental findings indicated that the positioning of the strain gauge had little impact. Overall, the computational method aligned well with the actual distribution

of residual stress and agreed with the experimental results. The study's findings can be considered reliable engineering data applicable in practical settings. Increasing voltage in welding simulations leads to higher levels of induced residual stresses, as the heat input energy, which is dependent on voltage, also increases. Similarly, increasing amperage in welding simulations causes an overall increase in input heat, increasing residual stress levels in welded structures and changing the temperature distribution, assuming constant linear welding speed and other variables.

Vemanaboina et al. (2020) [41] conducted a study on the multipass GTAW welding of SS316L. The weldment displayed good welds at temperatures above melting points and was devoid of flaws. Between the second and third passes, they successfully resolved faults related to hot cracking by integrating interpass temperatures. The results were nicely matched by the a priori thermal and mechanical boundary conditions. Peak temperatures in the weldment varied by 7.24%, as determined by infrared thermography and modelling. From X-Ray diffraction, residual stresses were shown to be symmetric and bell-shaped. By incorporating a safety margin of 1.025, the combined examination indicated that the distribution of maximum stress remained within acceptable limits, ensuring structural durability. Following the final iteration, a comparison between residual stress measurements and ANSYS simulation indicated a disparity of 16.66%. The authors recommend utilizing a higher heat input during the initial pass to achieve a thorough blending of the base and filler materials. Subsequently, for the second and third runs, the heat input should be reduced while retaining interpass temperatures to minimize temperature fluctuations and residual stress peaks.

Sojitriya et al. 2015 [42] conducted a study on predicting temperatures during the Single Pass Shielded Metal Arc Welding (SMAW) procedure. Utilising the finite element analysis programme ANSYS, the study involves doing a 3D thermal analysis of the SMAW procedure. The study employed Goldak's dual ellipsoidal heat source model, simulated the filler material through the element birth and death method, and considered thermal and mechanical properties that vary with temperature. Two K-type thermocouples were utilised in an experimental setup to validate the numerical model. The numerical analysis's findings closely matched the experimental data, showing that the proposed model's ability to forecast temperature distribution during welding was successful. Notably, there was a noticeable temperature gradient close to the weld bead and a nonlinear declining pattern in the temperature distribution along the transverse direction.

Pandi et al. (2014) [43] performed a thermomechanical finite element analysis to evaluate the residual stress in butt weld joints of AA7075 aluminium alloy. In order to determine the temperature distribution and heat flux in a plate measuring 300x300x6mm, they utilized ABAQUS for a basic thermal analysis. By considering heat generation, temperature distribution, and residual stress, they developed a three-dimensional finite element model to simulate the butt-weld process. In comparison to experimental methods, this strategy is more affordable. The simulation results indicate that heat input and welding speed significantly influence the weld response. The study's main conclusions and findings are outlined below: Al-Cu-Mg alloy AA7075 was the subject of a computational finite element analysis of butt welding. Using AA7075 Aluminium plates, a method for butt-welding was devised. Increasing the welding speed reduces the induced stresses in the plate because faster welding leads to less heat absorption by the base metal, resulting in lower stress. Residual stress was estimated by changing welding current (50A to 60A) and adjusting welding speed (3, 3.5, and 4 mm/sec) using the birth and death element technique in finite element analysis.

Syukri et al. (2015) [44] conducted research to explore the APDL Graphical User Interface approach in thermal simulation for the Butt-joint SMAW process. The research focused on the weld specimen of carbon steel ASTM A36 for butt joint SMAW process, with the electrode E6013 chosen for the experiment. The study examined various welding parameters, including plate thickness (2, 4, 6) mm and welding speed (10, 12.5, 15, 17.5, 20, 22.5 25, 27.5, 30, 32.5) mm/sec, Employing the ANSYS software, an investigation is conducted to showcase the influence of various welding parameters on the plate as it undergoes the joining procedure. The analysis of the thermal simulation yielded several conclusions, including the determination of optimal welding speeds for different metal thicknesses. Additionally, the simulation results provided evidence that thinner metal plates dissipate heat at a slower rate compared to thicker plates, necessitating higher welding speeds for satisfactory welding quality on thinner plates.

Shenbagavalli et al. (2020) [45] dynamically simulate the projection welding of steel sheets, research was conducted and a finite element model with three dimensions was produced. By altering the welding parameters and using a non-linear transient thermal analysis, a numerical simulation was carried out. For our study state thermal analysis, we used ANSYS 2022R2 to create a moving Gaussian-distributed heat source and calculate the temperature distribution on the nut and plate. Work plates and weld tool tips are successfully created and imported in 3D form for joining two similar types of steel. On the nut and plate, a finite element analysis is conducted. Temperature distribution and thermal flux are discovered through thermal analysis.

According to the findings, stage 3 has a higher thermal flux and temperature than stage 2. During stage 2, the maximum temperature recorded was 1375°C, accompanied by a heat flux of 42396 W/cm2. However, in stage 3, the maximum temperature reached was 1461.3°C, with a heat flux of 21609 W/cm2. The temperature achieved in stage 3 is deemed adequate to attain the melting points of the plates. According to the results of the FEA analysis, stage 3 of projection welding is preferred over stage 2. not clean up the burr during projection welding. not clean up the burr during projection welding. successfully fixed on the plate and nut by 95% projection welding.

Gohel et al. (2016) [46] conducted a study on the use of 304 austenitic stainless steel as the material for the existing work. The workpiece measures 120 mm x 50 mm x 3 mm. Argon gas was used as a shield. A symmetrical plate was created to study temperature distribution. The analysis considered a convection boundary condition while neglecting the radiative boundary condition. Experimental measurements of temperature were taken at distances of 10 mm, 20 mm, and 30 mm from the weld centre line. The numerical temperature profile was validated against the results obtained from ANSYS. The welding parameters used were current 70 A, voltage 20 V, and welding rate of 3.84 mm/sec. Based on simulation results, the temperature at the first distance of the node, which was 10 mm away from the welding centre line, showed that two temperatures a highest one of 180.54°C and a lowest one of 165°C had an impact on the results. 20 mm from the weld centre line, the second node distance, also revealed a highest temperature of 31.785°C and a lowest temperature of 30.176°C. At a distance of 30 mm from the weld centre line, the third node experienced two temperatures: a highest of 22.211°C and a lowest of 22.165°C. Temperatures at 10, 20, and 30 mm were respectively 168°C, 29.5°C, and 20°C higher than the experimental values.

# CHAPTER 3

# EXPERIMENTAL INVESTIGATIONS

In this chapter, the experiment focuses on studying welding techniques where the molten electrode metal is used to join workpieces by filling the weld gap. For welding stainless steel, specialized electrodes suitable for the specific marine grade of stainless steel are typically required. These electrodes are created to give the required mechanical properties and corrosion resistance in the welded joint while also matching the chemical composition of the base metal. Various welding parameters are adjusted to ensure proper heat input, preventing issues such as excessive heat distortion, grain growth, and metallurgical problems. The microstructure analysis involves examining the arrangement, composition, and characteristics of microscopic constituents within the weld. It also includes studying the phases present, grain structure, solidification structure, heat-affected zone, and detection of defects. To analyse these aspects, techniques such as optical metallurgical microscope and scanning electron microscope (SEM) are utilized. The mechanical properties of both the original material and the welded samples are assessed, focusing on microhardness, compressive properties, and tensile properties. ANSYS software was utilized to conduct thermal analysis and examine temperature fluctuations in different sections of the plate.

## 3.1 Work Materials

The SS316L austenitic stainless steel has been used as a base material (BM) for present study, which was obtained from the Metal World Kolkata, W. B, India. The welding process involved the use of filler materials, namely AWS A5.4 E316L-16 and AWS A5.4 E308L-16, which were sourced from Excellent Weld-Aids in Kottayam, Kerala, India. The detailed chemical composition of base alloy AISI 316L is shown in Table 3.1, and the chemical composition of filler materials, electrode E316L-16 and E308L-16 is shown in Table 3.2. In addition to the welding materials, cutting-off wheels and flap discs were also utilized. The chemical composition of both the base alloy and the filler materials is provided in the table below.

**Table 3.1:** Chemical composition of base alloy SS 316L.

| Base Alloy | Elements (wt.%) | | | | | | | | | |
|---|---|---|---|---|---|---|---|---|---|---|
| | C | Mn | P | S | Si | Cr | Ni | Mo | N | Fe |
| AISI 316L | 0.03 | 2.0 | 0.045 | 0.03 | 0.75 | 16.0 | 10.0 | 2.0 | 0.1 | Balance |

**Table 3.2:** Chemical composition of filler materials E316L-16 and E308L -16.

| Filler Materials | Elements (wt.-%) | | | | | | | | | |
|---|---|---|---|---|---|---|---|---|---|---|
| | C | Cu | Mo | Mn | Ni | Cr | Si | P | S | Fe |
| E316L-16 | 0.02 | 0.05 | 2.8 | 0.6 | 11.6 | 18.6 | 0.61 | 0.03 | 0.01 | Balance |
| E308L -16 | 0.03 | 0.03 | 0.02 | 0.7 | 9.7 | 19.4 | 0.78 | 0.02 | 0.01 | Balance |

## 3.2 Techniques Adopted for Welding of SS316L

The SS316L austenitic stainless steel is cut using a cut-off wheel to produce plates measuring 60 mm in length, 60 mm in width, and 2 mm in thickness. Once cut, the plates are filed using a stainless-steel flat file and a universal grinding machine to achieve the desired dimensions. A total of three sets of samples with identical dimensions are prepared. Before welding, the steel plate is polished with the help of emery paper to ensure flat edges. The SMAW technique is used for welding of SS316L steel using different filler materials (electrodes). The DCEN polarity is employed, where the electrode possesses a negative charge, while the workpiece is positively charged. Previously known as DCSP (direct-current straight polarity), this configuration is utilized. Using the SMAW technique, the samples are welded in the down-hand position at a 70-degree angle, employing a single square groove type weld. To reduce possible hazards, the welding safety measures ensured the proper utilization of personal protective gear, efficient ventilation, and adherence to safe work protocols throughout the welding process. The details welding procedure is shown in Figure 3.1.

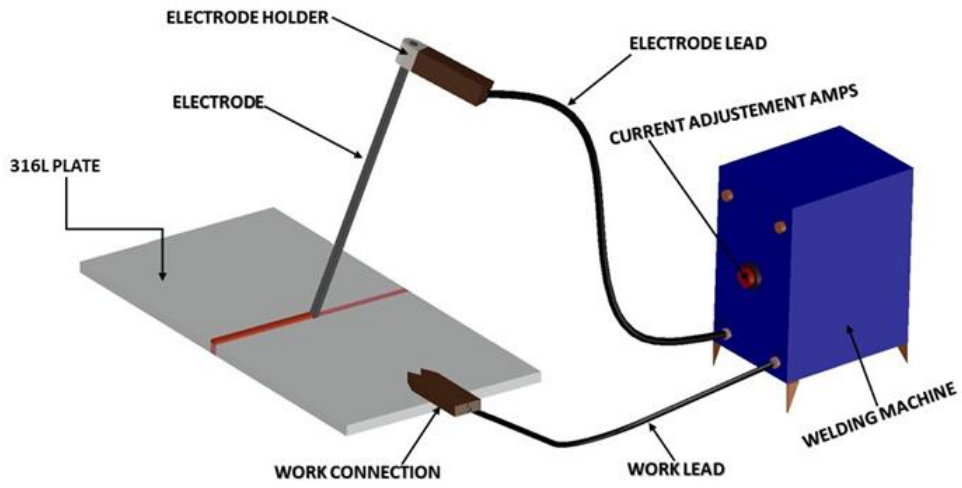


**Figure 3.1:** Schematic of SMAW Welding Techniques.

A varying current of 70 A, 80 A and 90 A with a constant voltage of 24 V was utilised to weld the specimen using (a) AWS A5.4 E316L-16 and (b) AWS A5.4 E308L-16 electrodes of 2.5 mm diameter as a filler material, arc length of 3 mm, and the number of passes is one. The detailed welding input parameter to weld the specimen using E316L- 16 (designated as A) and E308L– 16 (designated as B) filler material is shown in Tables 3.3.

**Table 3.3:** Welding input for specimen by using an electrode of E316L- 16 and E308L – 16 at various current.

| Sample (ID) | Welding Current (A) | Arc Voltage (V) | Weld length (mm) | Time (min) | Travel speed (mm/min) | Heat Input (KJ/mm) |
|---|---|---|---|---|---|---|
| A1 | 70 | 24 | 60 | 0.284 | 211.26 | 0.477 |
| A2 | 80 | 24 | 60 | 0.229 | 262.00 | 0.433 |
| A3 | 90 | 24 | 60 | 0.179 | 335.19 | 0.386 |
| B1 | 70 | 24 | 60 | 0.316 | 189.57 | 0.530 |
| B2 | 80 | 24 | 60 | 0.243 | 250 | 0.460 |
| B3 | 90 | 24 | 60 | 0.162 | 370.37 | 0.349 |

After successfully using the welding parameter the welded specimen prepares for further characterisation. Figure 3.2 shows the sample of (a) SS 316L plate before welding, and after the welding by using an electrode of (b) E316L-16, and (c) E308L-16 respectively.

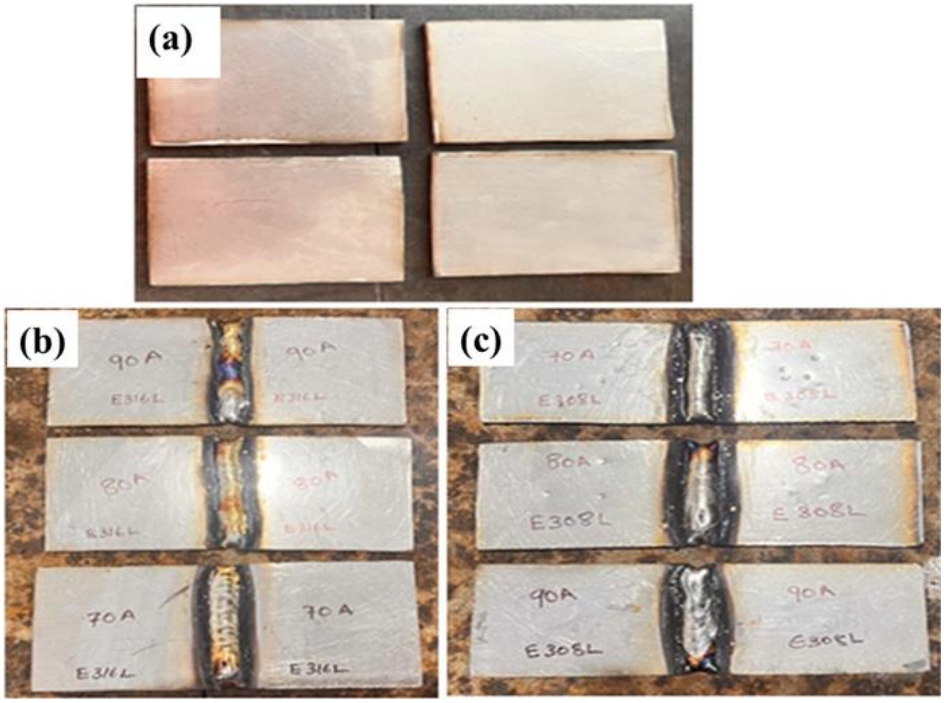


**Figure 3.2:** Photograph displays the preparation of samples (**a)** before welding after the welded samples using an applied current of 70 A, 80 A, and 90 and electrode of (**b)** E316L-16 and (**c)** E308L-16.

To calculate the heat input in Shielded Metal Arc Welding (SMAW), it is necessary to determine the amount of energy transferred to the workpiece per unit length by the welding arc [47].This can be achieved by applying the following equation.

$$\text{Heat input (HI)} = \frac{V \times I \times 60}{1000 \times S} \quad (1)$$

Where, HI is Heat Input in (kJ/mm), V is Arc voltage in volt, A is Welding Current in ampere, and S is Travel speed in (mm/min).

## 3.3 Characterization Techniques

After the successful welding of AISI 316L steel the effect of varying current and electrode on the microstructure and mechanical properties of the welded specimen has been characterised. Before conducting any characterization, a visual inspection was performed on the welded samples to detect any surface defects, cracks, or inconsistencies. Following the visual inspection, the prepared samples underwent a series of characterization techniques.

### 3.3.1 Microstructural Evolution

The optical microscopic examination was performed to understand the overall morphology of the welded samples. To analyse the microstructure, all the welded specimens were prepared following the standard ASTM E407. Epoxy resin was used to mount the surface and cross-

section of the samples, and they were then polished using various grades of emery paper, cloth, and diamond polishing to achieve a mirror finish. Following standard metallographic practices, the polished samples were etched with Kellings reagent ($CuCl_2$-5gm, HCL- 40 ml and Alcohol-40 ml). The microstructural characterization of representative samples was performed using an optical microscope Scanning Electron Microscope (SEM). SEM micrographs (Zeiss SMT AG) were used to examine the fusion zone (FZ), heat affected zone (HAZ) and any surface irregularities, aiding in the identification of features such as surface crack, inclusion or weld defects. Compositional analysis was performed using an Energy Dispersive Spectroscopy (EDS) system.

### 3.3.2. Microhardness

The hardness of the polished SS316L and the welded samples was measured using the Vickers micro-hardness tester). The measurements were taken on the base, heat-affected zone, and fusion zone. Before the hardness tests, the machine was calibrated using a standard test block of known hardness. The hardness measurement was started from one end of base region to second the end through HAZ and FZ. The average reading of welded zone was used to compare with the base material. The hardness was assessed under a normal load of 100 gf with a dwell time of 15 seconds.

### 3.3.3. Tensile Test

Transverse tensile specimens (length perpendicular to welding direction) were prepared using Electrical discharge machining (EDM) and evaluated in accordance with ASTM E8 standard for room temperature tensile tests. The sample design and dimensions for tensile tests at room temperature. Cross-head speed (displacement rate) of 1 mm/min was selected for tensile test. The 50 KN (Instron®: 8862) tensile testing apparatus used for the room temperature tensile tests. Figure 3.3 shows the dimension used to prepare a tensile specimen.

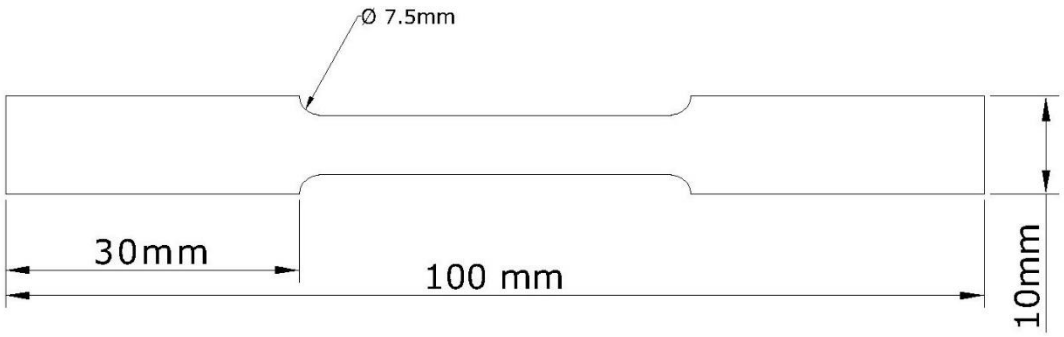


**Figure 3.3:** Dimension of Tensile welded specimen prepared by WEDM

## 3.4 Transient Thermal Analysis

In ANSYS, the process of conducting transient thermal analysis includes creating a finite element model of the object under study and determining the temperature distribution over time. The main steps involved in this procedure consist of (a) geometry creation, (b) meshing, (c) material assignment, (d) boundary condition definition, and (e) solution computation. By following these steps, a finite element model is generated, which enables the analysis of transient thermal behaviour and the acquisition of temperature distribution over time. The thermal analysis performed in this study employed the ANSYS 2023 R1 student version and encompassed all essential analyses within the transient thermal domain**.**

### 3.4.1 Finite Element Modelling for 316L

In transient thermal analysis, temperature field (T) of welded plate is a function of time (t). Thermal conduction will take place on the metal. The thermal equilibrium equation represents the governing partial differential equation for three-dimensional transient heat conduction with internal heat generation during welding is given by [48].

$$\frac{\partial}{\partial x}\left(\mathrm{K}_x \frac{\partial \mathrm{T}}{\partial \mathrm{x}}\right) + \frac{\partial}{\partial y}\left(\mathrm{K}_y \frac{\partial \mathrm{T}}{\partial \mathrm{y}}\right) + \frac{\partial}{\partial z}\left(\mathrm{K}_z \frac{\partial \mathrm{T}}{\partial \mathrm{z}}\right) + Q = \rho c \frac{\partial T}{\partial t} \quad (1)$$

Where, T represent the temperature (°C), K stand for thermal conductivity (W/m.°C),
c denotes the specific heat (J/kg°C), ρ represents the density (kg/m$^3$), t represents the time (min), Q represent the rate of heat generation per unit volume (W/m$^3$).
Boundary conditions, the specific heat flow acting over surface will be that of surface convection and radiation is given by [48].

$$\mathrm{K}_n \frac{\partial T}{\partial n} = h\left(T_w - T_f\right) + \varepsilon\sigma\left(T_w^4 - T_f^4\right) \quad (2)$$

where, h is the heat transfer coefficient at the model surface, Tw is the temperature of the model surface, $T_f$ is the temperature of the surrounding, ε is the radiation coefficient of the black body, and σ is the Stefan-Boltzmann constant.

The calculation of heat input in (SMAW) involves determining the quantity of energy transmitted to the workpiece per unit length by the welding arc. This is done by applying the following equation [47].

$$\text{Heat input (HI)} = \frac{V \times I \times 60}{1000 \times S} \quad (3)$$

where HI is Heat Input in (kJ/mm), V is Arc voltage in volt, A is Welding Current in ampere, and S is Travel speed (mm/min)

Heat Flux Equation can be calculated using this equation.

$$\text{Heat flux (q)} = \frac{H}{S \times L} \quad (4)$$

where q is Heat Flux in (W/mm$^2$), H = Heat Input in (joules/mm), S= welding Speed in (mm/s), L = length of the weld in (mm)

This equation relates the heat flux to the heat input, length of the weld, and welding speed. The heat flux is a measure of the amount of heat energy transferred per unit area per unit time, the heat input is the total amount of energy delivered to the weld area per unit length of the weld, and it is determined by the welding process parameters. Assuming that the heat input is uniformly distributed throughout the length of the weld and there are no heat losses, the equation enables the calculation of the heat flux, which can be utilized to approximate the temperature distribution in the material.

# CHAPTER 4

# RESULT AND DISCUSSION

## 4.1 Surface Micrograph Examination of the Welded Region

The surface micrograph and cross-section image of the SS316L welded plate by using electrode of E316L-16 (Figure 4.1 a-c and g-i) and E308L– 16 (Figure 4.1 d-f and j-l), and the current of 70 A, 80 A and 90 A are shown in Figure 4.1.

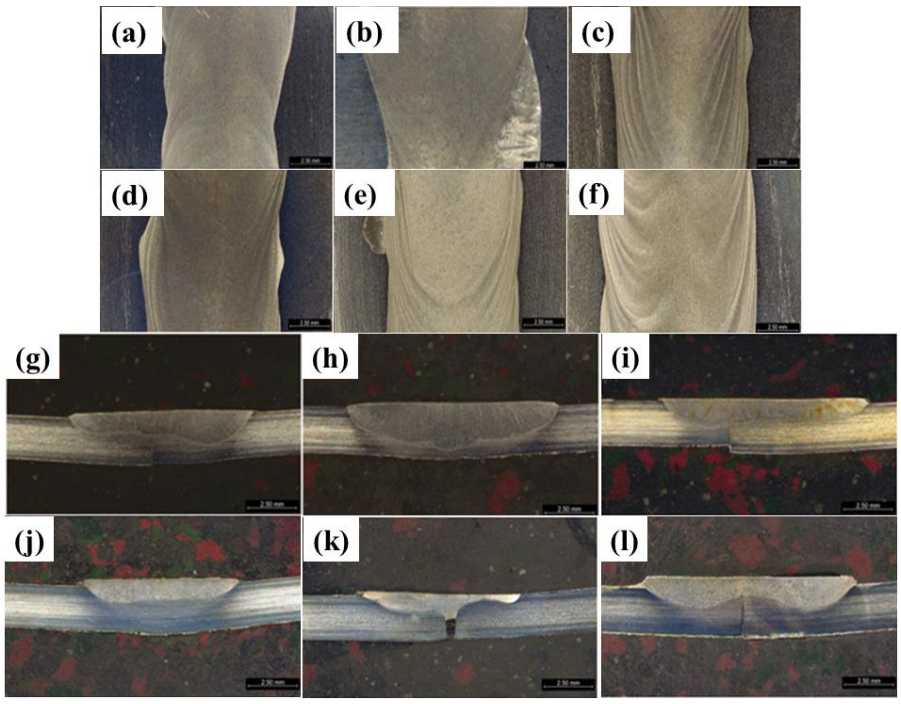


**Figure 4.1:** Surface micrograph and the cross-section image of SMAW welded SS316L using E316L-16 electrode (a-c and g-i) and E308L – 16 (d-f & j-l), at the applied current of 70 A, 80 A and 90 A respectively.

The weldment of SS316L plate using E308L-16 electrode showed that all specimens exhibited partial penetration due to the square butt joint. The same observation has also been observed in the welded plate using E308L-16 electrode. At 70 A, the weld pool's depth and width were small, and no imperfections were present. At 80 A, the weld pool had a small depth, but some gaps were observed in the lower region. The presence of a gap can be attributed to an incorrect or inconsistent electrode angle, which can cause uneven heat distribution and insufficient fusion. Similarly, inadequate fusion and the formation of gaps can result from improper joint

cleaning or the presence of gaps or inconsistencies in the joint configuration. The detailed process parameter is shown in Table 3.3. From the table it is observed that as the current increases from 70 A to 90 A the heat input decreases from 0.477 to 0.386 KJ/mm; however, the decrement in heat input is more for increase in current from 80 A to 90 A. Figure 4.1, shows the wideness of the welded zone increases as the current increases from 70 A to 80 A while further increase in current from 80 A to 90 A the welded zone and the depth of penetration decreases. As the current increases from 70 A to 80 A, the decrement in heat input is less which increases the time of surface melting and intermixing resulting increasing the depth of penetration. As the current increases from 80 A to 90 A, less depth of penetration is observed which possibly occurred due to the high welding speed, less intermixing and melting time. Overall, it has been observed that as the welding current increases, the width of the welded region increases and depth of penetration is decreases. This observation aligns with the comparison of welding parameter data, indicating that these factors contribute to changes in the macrostructure. Based on the findings, it can be concluded that an increase in welding current leads to an increase in welding speed for each specimen. Additionally, an increase in welding current results in a decrease in arc time and heat input on the weld region for each specimen.

## 4.2 Microstructure

Figure 4.2 shows the optical microstructure of (a) base alloy, and optical microstructure of SMAW welded SS316L alloy using an electrode of (c) E316L-16 and (e) E308L-16 respectively, and (b, d & f) is high magnification image of figure a, c, and d using 80 A current respectively. The microstructure of base material (SS316L) shows the presence of ferrite in austenitic matrix. Figure c and d shows the fusion zone & heat affected zone. In addition, the welded sample shows the fusion zone exhibited a microstructure consisting of a ferrite (dark) and austenitic (light) structure. The high magnification image (d and e) shows that the grains are finer and elongated along the heat decrement direction near the fusion zone.

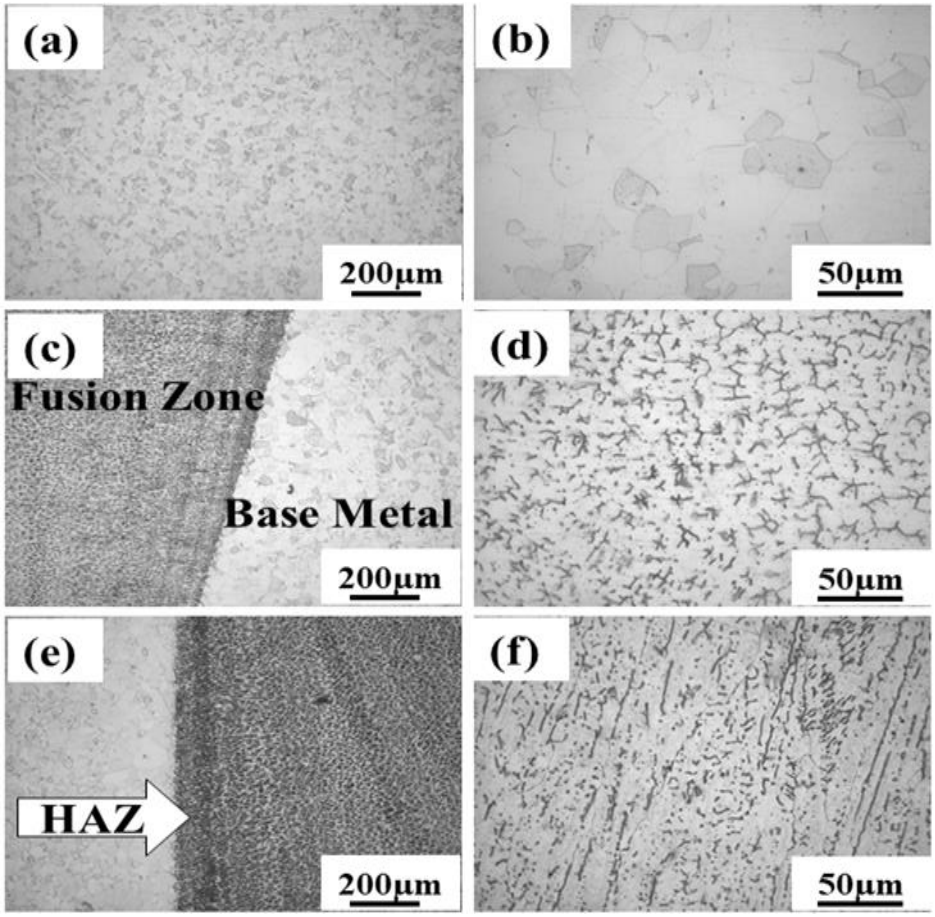


**Figure 4.2:** Optical microstructure of (a) base alloy, and optical microstructure of SMAW welded SS316L alloy using an electrode of (c) E316L-16 and (e) E308L-16 respectively, and (b, d & f) is high magnification image of figure a, c, and d using 80 A current respectively.

SEM microstructure of SMAW welded SS316L are shown in the Figure 4.3. Figure 4.3 a and c shows the welded specimen using an electrode of (a) E316L-16 and (c) E308L-16 respectively, and Figure 4.3 b and d shows the high magnification image of the Figure 4.3 a and c. From the SEM results, it has been observed that the weld beads obtained from two different electrodes showed clearly the welded and heat affected zone. The high magnification image shows there is presence of micro porosity that occurs due to the inclusion of residual gases in weld pool and after cooling these gases are trapped into the melt matrix resulting porosity. The porosity in welded sample might be observed because of no shielding gases, inadequate gas coverage, and possibly incorrect electrode angle. Additionally, the composition of the base metal, including elements or impurities such as sulphur, phosphorus, or carbon, can contribute to porosity formation.

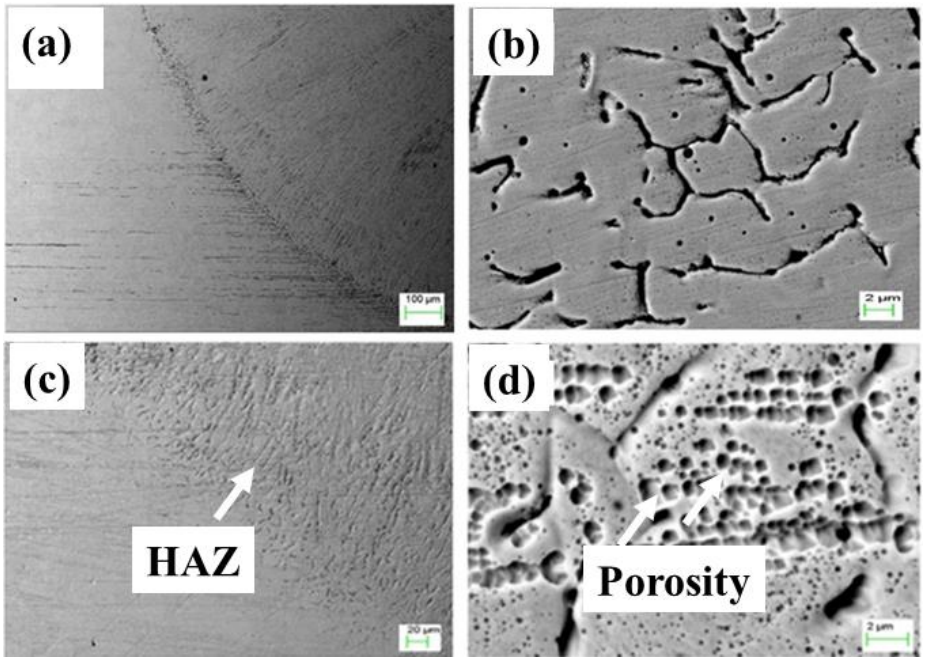


**Figure 4.3:** SEM microstructure of SMAW welded SS316L alloy using an electrode of (a) E316L-16, (c) E308L-16 respectively, and (b and d) is high magnification image of figure a and c, using 80 A current respectively.

The EDS spectrum images of welded zone is shown in Figure 4.4. Figure 4.4 a and b shows the EDS image of welded zone (using an electrode of E316L-16) and the presence of elements in respective zone. Similarly, the Figure 4.4 c and d shows the EDS image of welded zone (using an electrode of E308L-16) and the presence of elements in respective zone. The elemental analysis confirms that there is not the presence of any secondary element, oxides and carbides. The percentage of elements are showing similar pattern. Figure 4.4 c shows the high magnification of fusion zone showing porosity, and not presence of any other secondary phase in this region. The elevated Fe content is associated with an increased formation of ferrite in the microstructure. The presence of higher Fe content resultant ferrite formation in the weld samples depend on several factors, including the specific welding process and the composition of the base metal.

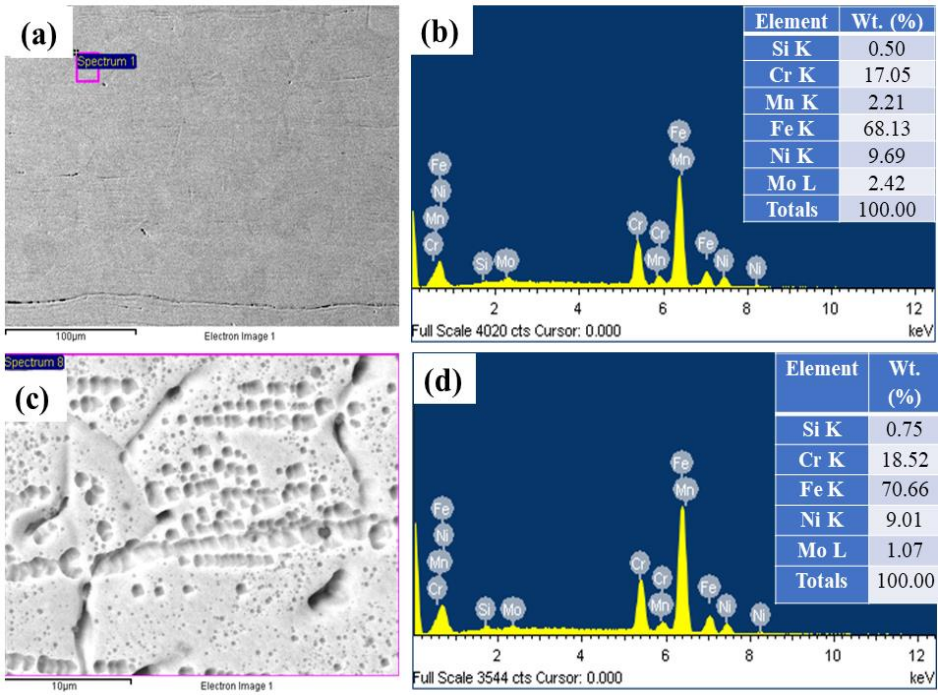


**Figure 4.4:** EDS spectrum images of welded zone using an electrode of (a) E316L-16 and (c) E308L-16, and (b and d) is showing the presence of elements (wt.%) in respective region.

## 4.3 Mechanical Properties

### 4.3.1 Microhardness

The Vickers microhardness profiles of welded samples using electrode E316L-16 & E308L-16 at an applied current of 70 A, 80 A and 90 is shown in Figure 4.5. The hardness has been taken from the one end of base region to second end of base region through the heat affected zone and welded zone at every 250-micron distance, to understand the hardness trend at base, FZ and HAZ region. From the figure it may be observed that the fusion zone (in the middle) exhibits higher hardness, which gradually decrease along the heat affected zone and the base sample. The higher hardness possibly occurs in the fusion zone due to fine grain structure. This phenomenon has also been attributed to the presence of electrode elements, variation in grain size, and the presence of ferrite structure within the internal composition of the SS 316L welds. The HAZ adjacent to the fusion boundary exhibits a fine grain size, resulting in higher hardness. Conversely, the HAZ adjacent to the base metal shows a coarser grain structure, leading to lower hardness values. The areas adjacent to fusion zone experience a relatively faster cooling rate, resulting in a finer-grained microstructure. On the other hand, the area adjoining the base metal undergoes a slower cooling rate. In general, the hardness

measurements indicate a decreasing trend in the weld metal and HAZ, following this order which is shown in Figure 4.5.

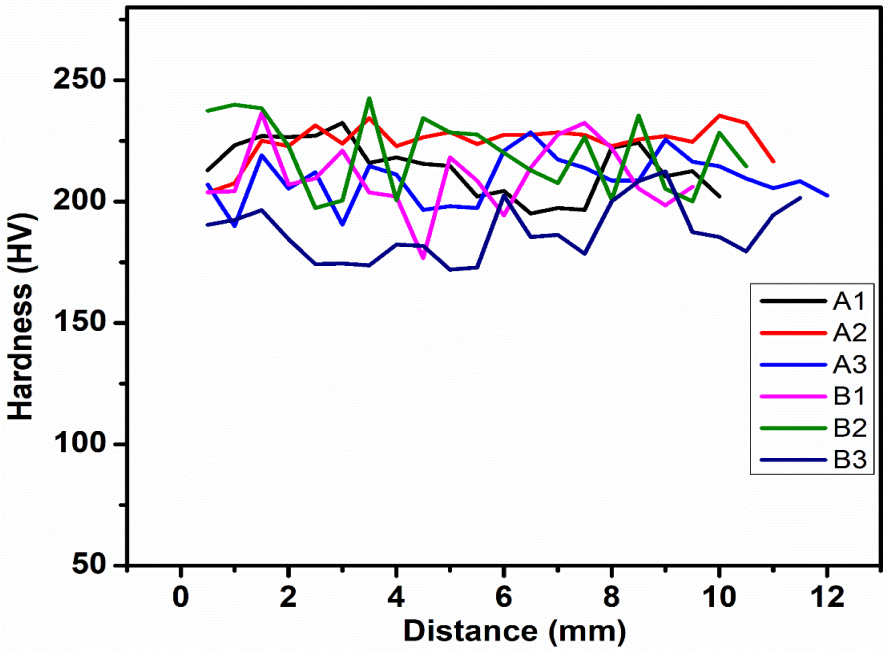


**Figure 4.5:** The hardness trend of welded samples using electrode E316L-16 (designated as A) & E308L-16 (designated as B) and current of 70 A (A1 and B1), 80 A (A2 and B2) and 90 A (A3 and B3) at the fixed distance.

The hardness at the fusion zone has been taken in both the samples and the average of 15 readings has been taken to draw a bar graphs which is shown in Figure 4.6. From the bar graphs, it can be observed that the welded using E316L-16 electrodes displayed greater hardness compared to those welded using the E308-16 electrodes. It was also noted that among all the samples, as the current is increasing the hardness at the fusion zone increasing. The welded sample A2 (E316L-16 and current 80 A) shows a highest value of 223.38 HV compared to other welded samples. This could be attributed to the lower heat input and higher welding speed. As a result, the width of the weld pool increased, as observed in the macro structure, and the less penetration was also consistent in both samples.

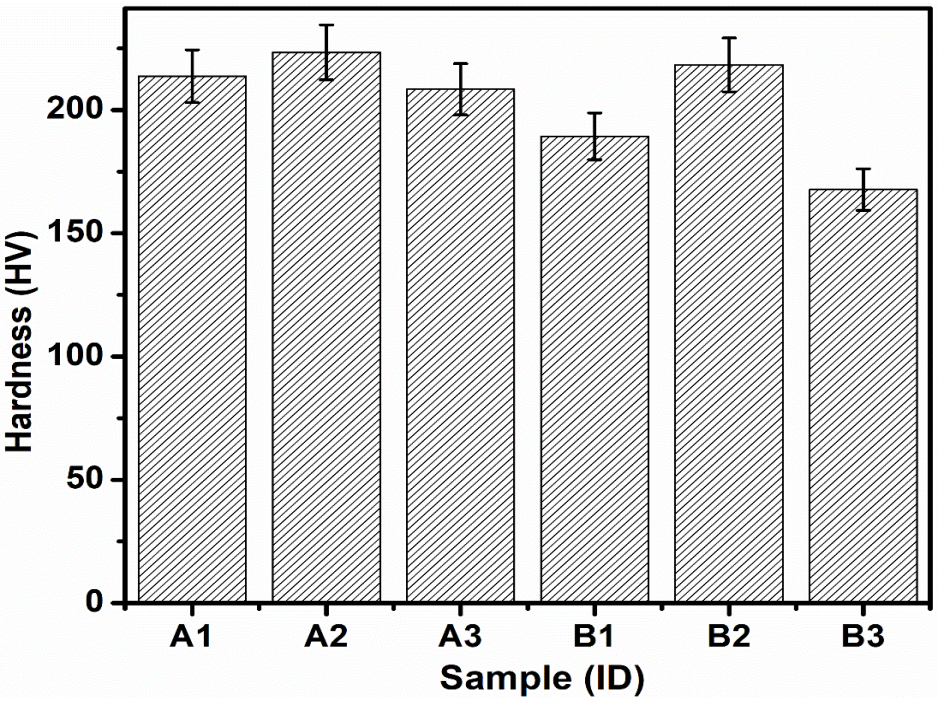


**Figure 4.6:** The diagram shows the hardness of fusion zone of welded samples using an electrode of E316L-16 and E308L-16 and current of 70 A, 80 A and 90 A.

### 4.3.2 Tensile strength

Tensile testing was performed on all the welded samples to study the relationship between applied stress and strain which is shown in Figure 4.7. The graph depicts the tensile stress versus tensile strain, with the x-axis representing the applied strain (fractional change in length) and the y-axis representing the corresponding tensile stress (force per unit area). As the stress increases, the material reaches the yield point, where it undergoes plastic deformation and does not fully regain its original shape upon stress removal. The strain increases more rapidly than the stress during this phase. Beyond the yield point, the material enters the plastic region. In this region, the graph shows a gradual and nonlinear increase in stress with strain. The material continues to deform plastically, and the strain increases at a relatively constant rate. This leads to permanent deformation. After reaching the peak, the stress begins to decline before the material ultimately fails or fractures. The stress at which fracture occurs is ultimate tensile strength (UTS), representing the maximum stress the material can withstand before failure. At this point, the material starts experiencing necking, resulting in narrowing and eventual fracture. The figure shows that the base sample exhibited the highest yield stress compared to all the welded samples. The detailed tensile results, i.e., yield strength, ultimate tensile strength and elongation percentage are demonstrated in Table 4.1.

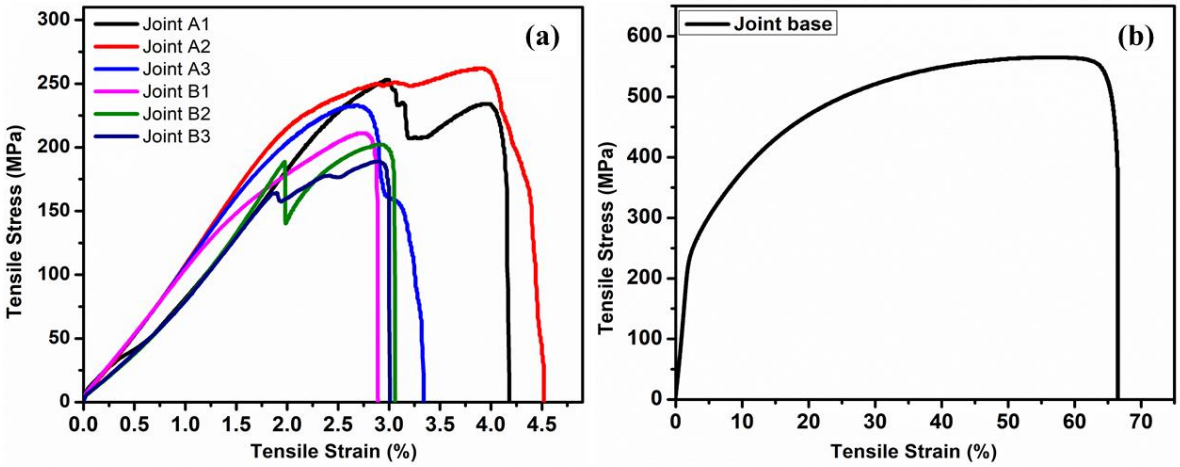


**Figure 4.7:** The diagram shows the Tensile stress vs strain graph of welded sample using an electrode of E316L-16 and E308L-16 and current of 70 A, 80 A and 90 A.

The tensile test results shows that the yield strength for E316L-16 electrode welded sample is decreasing from 253 N/mm$^2$ to 232 N/mm$^2$ and for E308L-16 electrode welded sample decreasing from 211 N/mm$^2$ to 164 N/mm$^2$ by increasing the welding current of 70 A to 90 A. However, the ultimate tensile strength of welded sample first increasing from 253 to 262 N/mm$^2$ as welding current increasing from 70 A to 80 A and further increasing in current from 80 A to 90 A it decreasing to 233 N/mm$^2$. The similar trend has also been observed for the E308L-16 electrode welded sample.

**Table 4.1:** Hardness of SMAW welded SS316L alloy using an electrode of E316L-16 and E308L– 16 at the applied current of 70A, 80A, and 90A.

| Sample (ID) | Hardness (HV) | Yield stress (N/mm$^2$) | Elongation (%) | Ultimate Tensile stress (N/mm$^2$) |
|---|---|---|---|---|
| Base | 212 | 552 | 42 | 565 |
| A1 | 214 | 253 | 3.1 | 253 |
| A2 | 223 | 246 | 2.8 | 262 |
| A3 | 208 | 232 | 2.6 | 233 |
| B1 | 190 | 211 | 2.7 | 211 |
| B2 | 218 | 189 | 2.0 | 202 |
| B3 | 168 | 164 | 1.9 | 190 |

The increasing in UTS with increasing in applied current occurs due to higher depth of penetration and uniform intermixing at the welded region while 90 A applied current has lower

strength because of lower depth of penetration and higher welding speed. The microstructure also confirms that the higher current has less depth of penetration and relatively higher trapped porosity. The elongation percent of all the welded sample varies from 1.9 to 3% which is lower compared to the base material. The tensile results confirmed that the mechanical strength of the welded sample depends on the welding parameter and welding technique.

## 4.4 Methodology of Thermal Analysis

The thermal analysis of welded zone was carried out using ANSYS 2023 R1 student version. For thermal analysis all the necessary analyses have been carried out in the transient thermal domain.

### 4.4.1 Geometry Creation

The geometry of the model was generated using the design modeler in ANSYS. The experiment involved two different dimension plates for two different electrodes. The first model consisted of two plates measuring 60 mm x 60 mm x 2 mm, which were welded together using SMAW techniques as depicted in the Figure 3.2. To represent the welding area, a half-circle with a diameter of 1 mm was incorporated into the models, and a penetration depth of 2 mm was included in the welded region. The entire model was constructed within ANSYS.

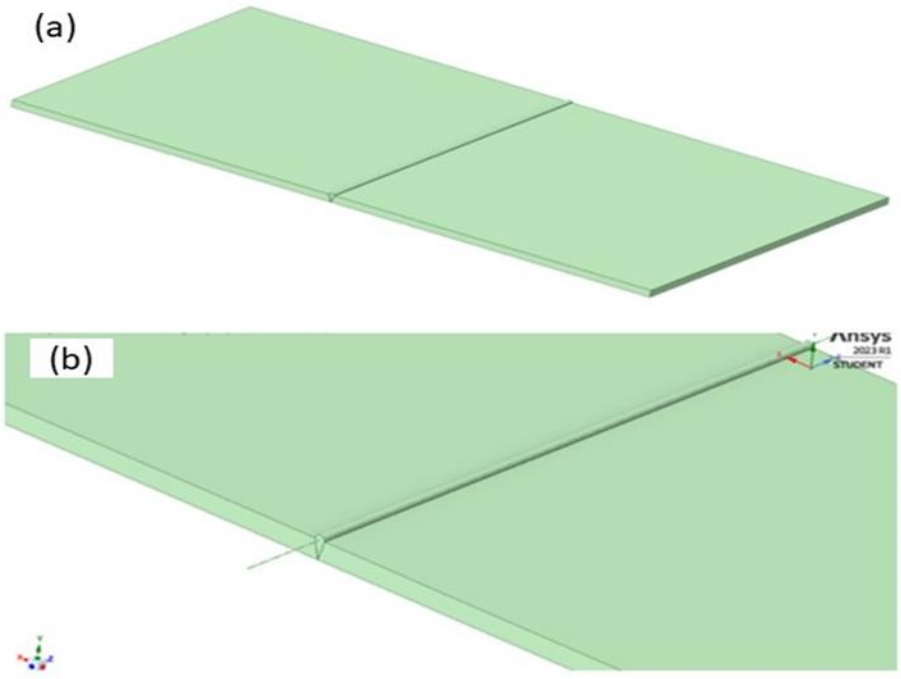


**Figure 4.8:** (a) The dimensions of the initial model are 60mm x 60mm x 2mm (b) Displays the side view of the welded region.

### 4.4.2 Meshing

The ANSYS default meshing provided in this model is sufficient for simple analyses due to its appropriate meshing. However, for more complex investigations, it becomes essential to customize and refine the mesh size in critical areas to enhance accuracy and achieve better results. The figure presented illustrates the usage of a refined meshing, indicating the model's geometry with excellent skewness, which signifies a well-optimized mesh using ANSYS's default meshing.

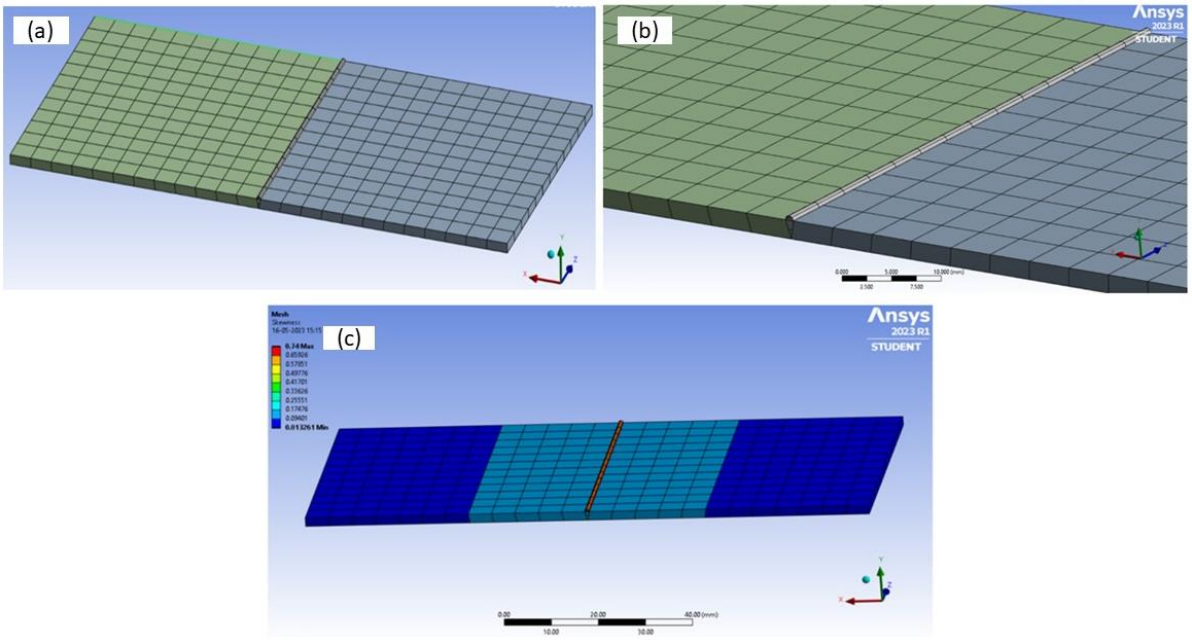


**Figure 4.9:** (a) Shows meshing, (b) showing the geometric area of welded region (c) shows the skewness meshing for welding specimen.

### 4.4.3 Material Assignment and Boundary Condition

SMAW techniques were employed to weld the stainless steel 316L material. The thermal and mechanical properties of the base material is shown in Table 4.2 [49]. These properties were subsequently inputted into Ansys engineering data to analyse the geometry of the two plates and the welded region. The plates and the welded region both utilized the same SS316L properties in the model, considering that the material melts during welding and forms a joint. An ambient temperature of 33°C has been set as a boundary condition for the transient thermal analysis. Both the plate body geometry has been assigned a convection heat coefficient, also known as the film coefficient, of 25.32W/ ($m^2$ K) for steel is considered. The heat flux obtained

from the calculation has been applied to the welded region based on the corresponding time required to complete the weld, determined experimentally.

**Table 4.2:** Thermal and mechanical properties of the base materials [49].

| Materials | Thermal Conductivity | Density | Specific Heat | Yield Strength | Poisson's Ratio | Coefficient of Thermal Expansion |
|---|---|---|---|---|---|---|
| Units | W/m K | $Kg/m^3$ | J/kg K | MPa | - | - |
| SS 316L | 21.26 | 7817 | 572 | 193 | 0.3 | $15.6^{e-6}$ |

### 4.4.4 Solution

Two different types of electrodes, namely the E316L-16 and E308L-16, were employed in the welding process. These electrodes were used to weld 316L material using the SMAW technique. The heat input and heat flux were determined by utilizing the welding parameters and equations (3) and (4). The analysis results are presented in the table below.

**Table 4.3:** The utilization of electrode E316L-16 & E308L-16.

| Specimen ID (A) | Current | Voltage | Welding Speed [mm/min] | Heat Input (kJ/mm) | Heat Flux ($W/mm^2$) |
|---|---|---|---|---|---|
| A1 | 70 | 24 | 211.26 | 0.477 | 2.25 |
| A2 | 80 | 24 | 262.00 | 0.433 | 1.65 |
| A3 | 90 | 24 | 335.19 | 0.386 | 1.15 |
| B1 | 70 | 24 | 189.87 | 0.530 | 2.80 |
| B2 | 80 | 24 | 250 | 0.460 | 1.86 |
| B2 | 90 | 24 | 370.37 | 0.349 | 0.948 |

Observations indicate that when specimen sample A is welded with electrode 316L-16, an increase in welding current corresponds to an increase in welding speed for all A specimens. This implies that the electrode spends less time in contact with the base metal, resulting in reduced heat input. For instance, when using electrode E316, specimen A1 with a current of 70A and a welding speed of 211.26 mm/min yielded the highest heat input value among all A samples, measuring 0.477 KJ/mm. However, at 90A, the welding speed increased to 335.39 mm/min, resulting in a lower heat input value of 0.386 KJ/mm. Consequently, this may reduce the size of the overall heat-affected zone (HAZ), potentially minimizing distortion and heat-related issues in the weldment, as observed in the macro structure of all A samples. Furthermore, the faster welding speed leads to quicker cooling of the deposited weld metal. This rapid cooling can influence the microstructure, potentially resulting in a finer grain

structure, as seen in the microstructure of A samples. This finer grain structure enhances the mechanical properties of the weld, including increased strength and toughness. Additionally, increasing the welding speed can reduce weld penetration, as observed in the macrostructure of all A samples, indicating partial penetration. This is due to the shorter duration of the arc in contact with the base metal, limiting the depth of weld penetration into the joint. Faster welding speeds often produce narrower and more elongated weld beads, which can affect the overall appearance of the weld. Similar results were observed in specimen samples of B, where electrode E308l-16 was used. Increasing the current also increased the welding speed, leading to a decrease in heat input. when using electrode E316, specimen A1 with a current of 70A and a welding speed of 189.87 mm/min yielded the highest heat input value among all A samples, measuring 0.530 KJ/mm. However, at 90A, the welding speed increased to 370.37 mm/min, resulting in a lower heat input value of 0.349 KJ/mm.

### 4.4.5 Temperature Distribution

The temperature distribution and the maximum and minimum temperatures on the welding plate were determined by analysing the specimen A1, along with various data obtained from the welding parameters and equations. These values were inputted into the transient thermal analysis in ANSYS. Temperature distribution on specimen (A1) with a current of 70 A welded by Electrode E316L-16 is shown in Figure 4.10.

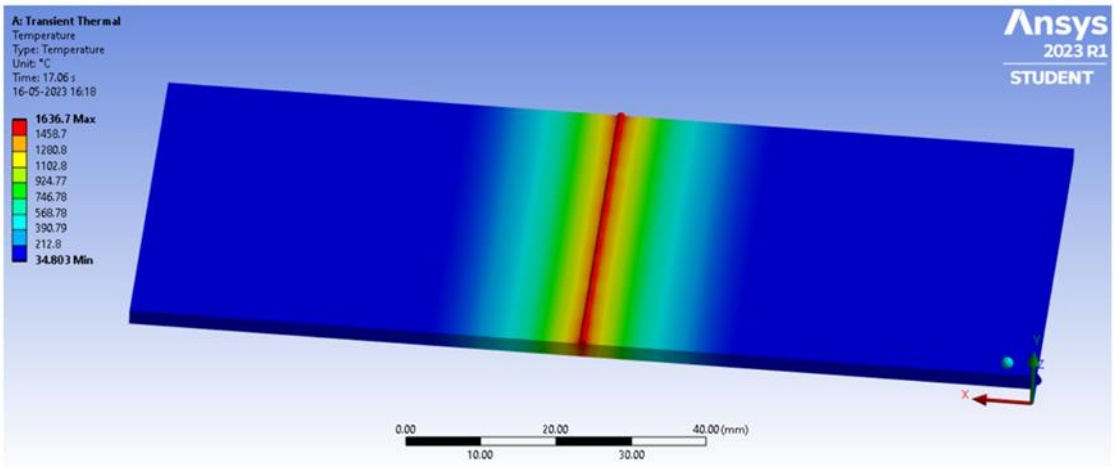


**Figure 4.10:** Temperature distribution on specimen (A1) with a current of 70A welded by Electrode E316L-16.

The figure illustrates the temperature distribution, typically represented using a colour map, where colours like blue or green indicate lower temperatures, transitioning through

intermediate colours like yellow or orange, and ultimately ending with a warmer colour like red to represent higher temperature regions. Furthermore, the figure demonstrates that the temperature decreases from the red-coloured welded region towards the blue-coloured area along the plate.

**Table 4.4:** Electrode Utilized for Specimen (A) is E316L-16 & E308L-16.

| Specimen ID (A) | Time (sec) | Maximum Temperature | Minimum temperature |
|---|---|---|---|
| A1 | 17.06 | 1636.7 | 34.803 |
| A2 | 13.74 | 1106.1 | 34.815 |
| A3 | 10.74 | 706.69 | 34.847 |
| B1 | 19.0 | 2121.3 | 34.837 |
| B2 | 14.62 | 1274.9 | 34.808 |
| B3 | 9.75 | 566.14 | 34.858 |

The heat flux applied at the welded region for specimen A1 is 2.25 W/mm$^2$. The corresponding welding time required to complete the welding is 17.06s. The analysis results show that the maximum temperature at the welding region reaches 1637.5°C, indicated by its red colour. On the other hand, the minimum temperature at the end of the plate is 34.806°C, represented by its blue colour. Table 4.4 shows the maximum and minimum temperature in welded sample using an electrode of E316L-16 & E308L-16analysis on the A1 and other remaining specimens of A2, A3, B1, B2, and B3. From the table it has been observed that the welding sample (A1) reached its highest maximum temperature at 1637.5, taking 17.06 seconds to complete the weld. On the other hand, the lowest temperature for (A2) was 706.69, with a completion time of 10.74 seconds. Similarly, in the case of welding sample (B1), the maximum temperature was 2121.3, and the completion time was 19.0 seconds. For welding sample (B3), the lowest maximum temperature recorded was 566.14 degrees Celsius, and the completion time was 9.75 seconds. It can be observed from both specimens that as time decreases, the temperature also decreases. This correlation is reflected in the heat input, where a shorter duration of the arc generates less heat. Generally, a longer welding time allows for a higher heat input, resulting in a higher temperature. Conversely, a shorter welding time limits the heat input and can lead to a lower temperature [50].

### 4.4.6 Correlation of Welding Temperature with the Microstructure

The temperature distribution from the centre region of the welded zone to base region of the welded sample using E316L-16 and E308L-16 and 80 A current is shown in Table 4.5.

**Table 4.5**: The distance and temperature of the specimen at different locations.

| Distance Location (mm) | 0.5 | 0.6 | 0.7 | 0.8 | 0.9 | 1 | 3 | 5 | 10 | 60 |
|---|---|---|---|---|---|---|---|---|---|---|
| A2 (Temp in °C) | 989.51 | 988.84 | 986.95 | 983.84 | 979.51 | 973.96 | 744 | 579.18 | 300.16 | 34.997 |
| B2 (Temp in °C) | 1143.2 | 1142.5 | 1140.4 | 1136.8 | 1131.9 | 1125.7 | 869.04 | 678.19 | 356.66 | 34.997 |

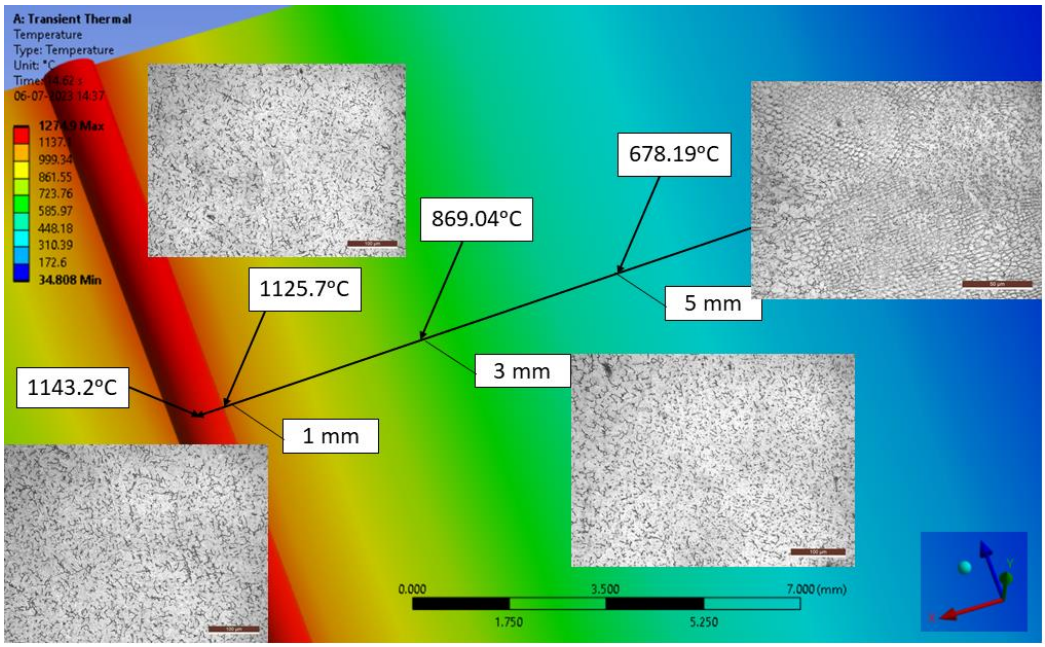


**Figure 4.11:** Temperature distribution of welded sample and microstructure at the respective distance using an electrode of E308L-16 and 80 A current.

From the table it is observed that the temperature decreasing from centre of welded zone to base region for both the samples. The temperature is more for the welded sample using an electrode of E308L-16 and 80 A current. The correlation of welding temperature with the microstructure at the respective distance using an electrode of E308L-16 and 80 A current is shown in the Figure 4.11. The figure shows that the temperature is highest in the welded region. Since, the cooling rate is maximum at this position resulting the fine grain microstructure has been observed. As the temperature decreasing the microstructure shows relatively coarser grain. The microstructure at the distance of 5 mm shows the heat affected zone and the respective microstructure confirms coarser grain structure compared to the welded zone.

# CHAPTER 5

# CONCLUSION AND FUTURE SCOPE

## 5.1 Conclusion

In the present study, SMAW welding process has been used to join SS316L using varying current (70 A to 90 A) and two different kinds of electrode (E316L-16 and E308L-16). The effect of process parameters on the microstructure, mechanical properties and temperature distribution in weldments with correlation with the microstructure has been studied. The following conclusions can be taken from the detailed analysis, and they are summarised below:

1. The applied current, welding speed, heat input, and properties of electrode affect the weld penetration. As the welding current increases the wideness of the welded zone first increases from 70 A to 80 A, while further increases in the current, welded zone and the depth of penetration decreases.
2. In the surface micrographs of all the samples, it was observed that by using an electrode of E316L-16 with an increased welding current, there was an increase in the width of the weld pool without any defects. However, when E308l-16 was used with a welding current of 80 A, a gap defect was identified which may attributed to presence of a gap and it depends on several factors such as incorrect or inconsistent electrode angle, leading to uneven heat distribution and inadequate fusion.
3. The microstructure shows, the finer grain structure at the welded zone, and coarser grain at the heat affected zone compared to base.
4. The hardness of weldment first increases with increasing in current from 70 A to 80 A due to finer grain structure; however, further increases in the current up to 90 A the hardness of the weldment decreases due to less higher welding speed and low intermixing. The microhardness test results revealed that both E316L-16 and E308L-16 exhibited their highest hardness at 80 A, with values of 223 HV and 218 HV, respectively.
5. The tensile test results show that the yield strength for E316L-16 electrode welded sample is decreasing from 253 $N/mm^2$ to 232 $N/mm^2$ and for E308L-16 electrode welded sample decreasing from 211 $N/mm^2$ to 164 $N/mm^2$ by increasing the welding current of 70 A to 90 A. However, the ultimate tensile strength of welded sample first

increased from 253 to 262 N/mm$^2$ as welding current increased from 70 A to 80 A and further increased in current from 80 A to 90 A it decreasing to 233 N/mm$^2$.

6. The thermal analysis of SS316L revealed that as the welding current increased, the time required to complete the weld decreased in all samples. Additionally, the temperature of both electrode samples decreased as the welding time decreased, as indicated by the simulation results. The temperature distribution of the samples along the plate was also observed in different regions.
7. The heat input and microstructure correlation confirm that the finer grain structure at near the welded zone (up to 1 mm distance from centre) and coarser at the heat affected zone (5 mm distance from centre).

## 5.2 Future Scope of the Research

In the present study though the SS316L weldment, characterization, and property evaluation has been made using varying current and electrodes; however, large numbers of studies need to be undertaken which was beyond the scope of the present investigation and may be summarized as follows:

(1) Corrosion and wear study of weldments needed for the application in ship structures.
(2) In future investigations, another marine grade material, welding technique, especially high energy beam welding will be incorporated along with the exploration of various parameters, including corrosion tests.
(3) Comparison of the cost and parametric study of the weldment fabricated by different processing routes.
(4) In upcoming experiments, advanced temperature measuring equipment such as K-type thermocouples, Fluke devices, and similar tools will be utilized for precise temperature measurement along the welded area and to evaluate its impact on the plate.
(5) Furthermore, a more comprehensive thermal analysis will be conducted using the APDL (Ansys Parametric Design Language), which allows sophisticated engineering simulations based on the Finite Element Method (FEM).

# REFERENCES


[1] S.K. Sharma, A.K. Singh, R.K. Mishra, A.K. Shukla, and C. Sharma, Processing Techniques, Microstructural and Mechanical Properties of Additive Manufactured 316L Stainless Steel: Review, *J. Inst. Eng. Ser. D*, 2023.

[2] M.F. McGuire, "Stainless Steels for Design Engineers," *Stainless Steels for Design Engineers*, 2008.

[3] Asad Yousaf, Riffat Asim Pasha,Ashfaq Muhammad, "Effect of Filler Materials on Mechanical Properties of Shielded Metal Arc Welded AISI 316L Austenitic Stainless Steel Joints," *Inter. Conf. on Adv in Mech. Eng,* 2021.

[4] Asibeluo I.S, Emifoniye E, "Effect of Arc Welding Current on the Mechanical Properties Of A36 Carbon Steel Weld Joints," *Inter. J. of Mech. Eng*, 2015.

[5] Pushp Kumar Baghel, "Effect of SMAW Process Parameters on Similar and Dissimilar Metal Welds". *Elsevier*, 2022.

[6] A. S. AbdelWanees,T. S. Mahmoud, I. M. Ibrahim, "Effect of Electrode Material on Microstructural And Mechanical Characteristics of AISI 304 Stainless Steels Plates Joined Using Shielded Metal Arc Welding," *Eng. Res. J (Erj),* 2020.

[7] M. Sohel, M. Panwala, S.A. Channiwala, And K.N. Srinivasan, Numerical Simulation of Transient Temperature In SMAW, *Am. Soc. Mech. Eng. Press. Vessel. Pip. Div. PVP*, 2010, (PART A), P 449–456.

[8] A.K. Shukla, D. Gond, and D. Puri, "Effect of Cold Working on Hot Corrosion Behavior of 9 Cr–1 Mo Ferritic Steel in 75 Wt% Na2SO4 + 25 Wt% K2SO4 Molten Salt Environment at 900 °C," *Transactions of the Indian Institute of Metals*, 2016, p 1049–1057.

[9] https://www.stripdrains.com.au/blog/316l-stainless-steel/.

[10] Muyiwa Adedapo Fajobi,Tolulope Roland Loto,Olugbemiga Oluleke Oluwole "Austenitic 316L Stainless Steel;Corrosion and Organic Inhibitor,*Trans. Tech. Publications Ltd* ,2021, Vol. 886, pp 126-132.

[11] Eda Turan,Tarık Koçal,Kaan Ünlügençoğl, "Welding Technologies In Shipbuilding Industry," *The. Online . J. Scie. Tech,* 2011,Vol 1, p4, www.tojsat.net.

[12] M. P. Groover, Fundamentals of Modern Manufacturing Materials,Processes, and systems, *4th,edition*, 2010 .

[13] J. Labanowski,K. Krzysztofowicz,K. Samson, “Investigations into the Tendency to Stress Corrosion of Joints Welded in Austenitic and Duplex Steels, *Welding International*,2007, 21 (7) 521–524.

[14] https://www.materialwelding.com/what-is-submerged-arc-welding.saw/?utm_content=expand_article

[15] I.M.W. Ekaputra, Sudi Mungkasi1,Gunawan Dwi Haryadi,Rando Tungga Dewa,Seon-Jin Kim, “The Influence of Welding Speed Conditions of GMAW on Mechanical Properties of 316L,” *MATEC Web of Conferences*, 2018, 159, 02009.

[16] https://www.researchgate.net/publication/228766972_welding_technologies_in_shipbuilding_industry.

[17] Javed Kazi1,Syed Zaid,Syed Mohd Talha,Mukri Yasir,Dakhwe Akib, “A Review on Various Welding Techniques”, *Inter. J. Modern. Eng. Research.(IJMER),* 2015, Vol.5, 2249-6645.

[18] Azadkumar Vegda,Pradipkumar Maheshwari,Sumit Bhingradiya,Kaushik Faldu, “Experimentation, Analysis and Optimization of TIG Welding Process For SS316l”,*Inter. J. Research. Applied. science. Eng. Tech,* 2018, Vol 6.

[19] https://www.sciencedirect.com/topics/engineering/gas-tungsten-arc-welding.

[20] https://www.vssut.ac.in/lecture_notes/lecture1423905376.pdf.

[21] Jakub Kowalski,Łukasz Licznerski,Milena Supernak-Marczewska Krzysztof Emilianowicz1, “Influence of Process of Straightening Ship Hull Structure Made of 316l Stainless Steel on Corrosion Resistance and Mechanical Properties,” *Polish* Maritime *Research* 4 (108) ,2020 ,Vol. 27, pp103-11.

[22] https://www.engineeringnotes.org/welding/oxy-acetylene-gas-welding/.

[23] Ramazan Yılma,Mustafa Tümer,“Microstructural Studies and Impact Toughness of Dissimilar Weldments Between AISI 316 L and AH36 Steels by FCAW,” *Int. J. Adv Manuf. Technol ,*2013, 67, 1433–1447.

[24] https://shipjournal.co/index.php/sst/article/view/23/136.

[25] S.K. Sharma, A.K. Singh, R.K. Mishra, A.K. Shukla, and C. Sharma, Processing Techniques, Microstructural and Mechanical Properties of Additive Manufactured 316L Stainless Steel: Review, *J. Inst. Eng. Ser. D*, 2023.

[26] C.A.Walsh,“Laser Welding-Literature Review” M*aterials Science and Metallurgy Department*, University of Cambridge, England,2012.

[27] https://www.researchgate.net/figure/laser-welding-set-up-schematic_fig1_227222224.

[28] B. R, Kumar,N. Chauhan,P.M. Raole, “Mechanical and Microstructural Characterization of 8 mm Thick Samples of SS 316L by $CO_2$ Laser Welding,” *Advanced Materials Research*, 2012, Vol. 585 pp 430-434.

[29] https://eduengineering.wordpress.com/2015/01/10/proses-welding-smaw-shielded-metal-arc-welding/.

[30] Ugur Soy,O.Iyibilgin,Fehim Findik,Cemil Ozyasar Kiyan,“Determination of Welding Parameters for Shielded Metal Arc Welding” *Scientific Research and Essays*, 2011,Vol. 6(15), pp. 3153-3160, http://www.academicjournals.org/SRE.

[31] Mr. Mane Sambhaji B,Prof. Rajput A.D,Prof. Shitole J.S, “The Experimental Analysis of Various Parameter of Shielded Metal Arc Welding Validation of Taguchi Method,” *Inter. J. Adv. Res. Innovative. Ideas. Edu*,2021,Vol-7,2395-4396.

[32] Larry Jeffus, “Welding And Metal Fabrication”,2006.

[33] M. Mosaad,S. Mohamed, “Effect of Electrode type on the Characteristics of AISI 316 Stainless Steel,” *Eng. Research. J, (Erj),* 2020, Vol. 1, No. 44, pp5-9.

[34] Salman B.A,H. M. Ali, S.S. Mohammed, “Influence of Welding Process and Electrode Material on the Corrosion Characteristics of AISI 304 and AISI 316 Weldments,” *Eng. Research. J, (Erj),* 2020, Vol. 1, No. 45,pp. 7-12.

[35] L.O. Osoba, W.A. Ayoola, Q.A. Adegbuji, and O.A. Ajibade, Influence of Heat Inputs on Weld Profiles and Mechanical Properties of Carbon and Stainless Steel, *Niger. J. Technol. Dev.*, 2021, 18(2), p 135–143.

[36] A. S. AbdelWanees,T. S. Mahmoud, I. M. Ibrahim, "Effect of Electrode Material on Microstructural and Mechanical Characteristics of AISI 304 Stainless Steels Plates Joined Using Shielded Metal Arc Welding," *Eng. Res. J (Erj),*2020.

[37] Asad Yousaf,Riffat Asim Pasha,Ashfaq Muhammad, “Effect of Filler Materials on Mechanical Properties of Shielded Metal Arc Welded AISI 316L Austenitic Stainless Steel Joints,” *Inter. Conf. Adv. Mech. Eng*, 2021.

[38] E. Zumelzu,J. SepuLveda,M. Ibarra, “Influence of Microstructure on The Mechanical Behaviour Of Welded316 L SS Joints,” *J. Mater. Proces. Techno.*1999, Vol.94, P36-40.

[39] Apurv Choubey,Vijaykumar S. Jatti, “Influence Of Heat Input On Mechanical Properties And Microstructure Of Austenitic 202 Grade Stainless Steel Weldments,” *WSEAS Transactions on applied and Theoretical Mechanics,* 2014 , Vol.9, 2224-3429.

[40] S.S.Miftin,H.M.Mohammed,Ameen Ahmed Nassar, “Measurement and Prediction of Residual Stresses in Low Carbon Steel Pipes Welded Shielded Metal Arc Welding,” *Basrah. J.Eng.Sciences,* 2020, Vol. 20, No. 2, 60-65, www.bjes.edu.iq.

[41] H. Vemanaboina, S. Akella, A.C. Uma Maheshwer Rao, E. Gundabattini, and R.K. Buddu, Analysis of Thermal Stresses and its Effect in the Multipass Welding Process of SS316L, *Proc. Inst. Mech. Eng. Part E J. Process Mech. Eng.*, 2021, 235**(**2), p 384–391.

[42] Kalpeshkumar Sojitriya,Dr. V. D. Kalyankar, "Predictions of Temperature Distributions In Single Pass Shielded Metal Arc Welding Process,"*Inter. Conf. Adv. in Materials. Manuf. App* , 2015.

[43] M. Pal Pandi, Dr. R. Kannan, "Thermal Analysis on Butt Welded Aluminium Alloy AA7075 Plate using FEM," *Inter. J. Eng. Research,* 2014, Vol.3, No.2, pp116-120.

[44] Muhamad Safuan Bin Syukri, "Thermal Simulation of Different Welding Speed and Metal Thickness For Butt-Joint Welding With ANSYS,"2015.

[45] P. Shenbagavalli,A Gokul Rajan,B Pradesh Kumar,R Gnanaprakash, "Thermal Analysis of Projection Welding,"*Inter. Research. J. Eng. Techno,* 2022, Vol.09, p 2395-0072.

[46] Vijay Gohel,Jatin Makwana,Riteshkumar Ranjan, "Thermo-Mechanical Analysis In TIG Welding Of S.S 304," *Inter. J. Eng. Develop. Research,* 2016, Vol.4, 2321-9939.

[47] L.O. Osoba, W.A. Ayoola, Q.A. Adegbuji, and O.A. Ajibade, Influence of Heat Inputs on Weld Profiles and Mechanical Properties of Carbon and Stainless Steel, *Niger. J. Technol. Dev.*, 2021, 18(2), p 135–143.

[48] S.S.Miftin,H.M.Mohammed,Ameen Ahmed Nassar, "Measurement and Prediction of Residual Stresses in Low Carbon Steel Pipes Welded Shielded Metal Arc Welding," *Basrah. J.Eng.Sciences,* 2020, Vol. 20, No. 2, 60-65, www.bjes.edu.iq.

[49] H. Vemanaboina, S. Akella, A.C. Uma Maheshwer Rao, E. Gundabattini, and R.K. Buddu, Analysis of Thermal Stresses and its Effect in the Multipass Welding Process of SS316L, *Proc. Inst. Mech. Eng. Part E J. Process Mech. Eng.*, 2021,235(2), p 384–391.

[50] Vijay Gohel,Jatin Makwana,Riteshkumar Ranjan, "Thermo-Mechanical Analysis In TIG Welding Of S.S 304," *Inter. J. Eng. Develop. Research,* 2016, Vol.4,2321-9939.

[51] K.Dutta, Prof. S,"Different Types and New Applications of Stainless Steel," Vol.62 No.5, 2018.

[52] https://www.thoughtco.com/type-316-and-316l-stainless-steel-2340262.

[53] Prof. Rohit Jha, Dr. A.K. Jha, "Influence of Welding Current and Joint Design on the Tensile Properties of SMAW Welded Mild Steel Joints,"*Inter. J. Eng. Research. App*, 2014,Vol. 4, pp.106-111.

[54] M. Samir. Y, "Investigation on Effect of Heat Input on Cooling Rate and Mechanical Property (Hardness) of Mild Steel Weld Joint by MMAW Process," Inter. J. Modern. Eng. Research, 2015, Vol.5,2249-6645.